Remote Sensing Applications: Society and Environment 34 (2024) 101182

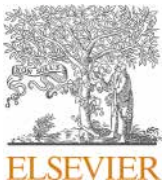

Contents lists available at ScienceDirect

Remote Sensing Applications: Society and Environment

journal homepage: www.elsevier.com/locate/rsase

Lake Tanganyika basin water storage variations from 2003–2021 for water balance and flood monitoring

Paul Gérard Gbetkom [a, *], Jean-François Crétaux [a], Sylvain Biancamaria [a], Alejandro Blazquez [a], Adrien Paris [c, a], Michel Tchilibou [a, 1], Laetitia Gal [c, a], Benjamin Kitambo [a], Rômulo Augusto Jucá Oliveira [c, a], Marielle Gosset [b]

[a] LEGOS, Université de Toulouse, IRD, CNES, CNRS, UPS, Toulouse, France
[b] GET, Université de Toulouse, IRD, CNES, CNRS, UPS, Toulouse, France
[c] Hydro Matters, 1 Chemin de la Pousaraque, 31460, Le Faget, France

ARTICLE INFO

Keywords:
Lake Tanganyika
Water storage
Rainfall
Flood
Spatiotemporal changes

ABSTRACT

Lake Tanganyika in East Africa contains 17% of the free freshwater on the Earth's surface and provides important ecosystem services to ~13 million people in the region. It is one of the great lakes in East Africa for which a significant rise in water level between 2019 and 2020 led to flooding, with major environmental consequences and social impacts. This study focused on the Lake Tanganyika basin water balance between 2003 and 2021 to assess the influence of recent climate variability on lake water level variations (due in particular to the floods of 2020 and 2021) and to explore early warnings of flooding in the lake's surrounding lowlands. This process is performed using remote sensing data. For the computation of the basin's water balance, we compared variations in the watershed total water storage (TWS) with the basin water flux calculated using rainfall, evaporation (E), evapotranspiration (ET) and discharges data. The space–time variations in rainfall, E and ET were analyzed by decomposing their time series into trend and seasonal signals and applying (only for rainfall) multivariate statistical analysis to the decomposed signals. For flood mapping, we calculated the MNDWI spectral water index from Sentinel–2 images acquired between 2017 and 2022. Our study showed that the basin water balance is closed when rainfall from Era5 is combined with E and ET from GLEV and MOD16A2, respectively. During the 2003–2021 period, over the entire watershed, water losses of ~70 km^3 due to lake E were offset by an increase in water inflows of ~100 km^3 in the rest of the watershed. During the period from 2003 to 2021, the E rate from the lake was stable overall, while the ET and rainfall mainly in the Malagarasi basin increased significantly. The surface water storage (SWS), which represents the variation in lake water volume derived from altimetry measurements, corresponds to 41.8% of the TWS, groundwater storage corresponds to 57.7% of the TWS, and the soil moisture is less than 0.5%. The TWS strongly correlated with the SWS (~91%), with a one-month lag in the SWS variations in response to the TWS fluctuations. Therefore, the SWS in May, when the flood risk is the highest, was estimated using TWS in February, March and April with accuracies of 85%, 94% and 95%, respectively. This valuable information could be integrated into flood management tools, particularly for areas such as Gatumba city and the Ruzizi Delta Nature Reserve, which were heavily affected by the May 2021 floods.

* Corresponding author.
E-mail address: paul-gerard.gbetkom@univ-tlse3.fr (P.G. Gbetkom).
[1] Present address, Collecte Localisation Satellites SA, Ramonville saint agne, France.

https://doi.org/10.1016/j.rsase.2024.101182
Received 27 December 2023; Received in revised form 16 February 2024; Accepted 26 February 2024
Available online 28 February 2024

1. Introduction

Lakes and their associated ecosystems are valuable physical environments for understanding the planet response to climate change (Pan and Yang, 2021; Torabi Haghighi and Kløve, 2015; VanDeWeghe et al., 2022; Wang et al., 2023). They contain 87% of the Earth's liquid surface freshwater (Carrea et al., 2023; Woolway et al., 2020). In addition, variables such as lake surface water temperature, water level and extent, ice cover and lake color are now listed as essential climate variables (ECVs) and are used as key factors in studies describing the Earth's climate (Carrea et al., 2023; Woolway et al., 2020). For example, Yao et al. (2023) studied the lake water storage (LWS) of the 1972 largest lakes in the world over the period 1992–2020 and found that 53% of them experienced significant volume declines. These authors attributed these volume losses to climate warming, increased E and human needs in the case of natural lakes and to sedimentation in the case of reservoirs. Woolway et al. (2020) noted that, in some regions of the world, the lake surface water temperature (LSWT), responded to climate change faster than the overlying air temperature did. For example, Dokulil et al. (2021) observed an increase in the maximum lake surface temperature of ~ +0.6 °C/decade for ten lakes in Europe between 1966 and 2015. They found that this trend was coupled with an increase in the maximum annual air temperature of ~ +0.42 °C/decade over the same period. Xie et al. (2022) reported an average increase of 0.26 °C/decade in the LSWT of 169 large lakes across China during 2001–2016 and observed a positive correlation between the LSWT and air temperature trends over this period. Therefore, they stated according to their results that lake temperature variations can be linked to geographical location and topography. Lakes are also sensitive indicators of climate change at the regional scale. For example, in the Eurasian Endorheic Lakes, monitoring of the surface water level (SWL) and LWS during 1990–2020 indicated a decreasing trend in lake levels in Central Asia and the Mongolian Plateau (Huang et al., 2022; Zhang et al., 2021). On the entire Tibetan Plateau, the overall LWS increased by ~110 Gt from the 1970s to 2015 (Zhang et al., 2020). In addition, other regional studies have shown a reduction in the water level and volume of Lake Egirdir over the period 1988–2019 (Yücel et al., 2022), a decreasing trend in the water level of Lake Urmia for the period 1966–2012 (Fathian et al., 2014), or an increasing trend in the water levels of the Great Lakes in the 2013–2020 period (Kayastha et al., 2022).

In the East African Great Lakes region, Khaki and Awange (2021) observed a significant increase of ~1.4 m in Lake Victoria's SWL during 2019–2020 compared with its mean level during 2002–2018. This resulted in a significant increase in the estimated water storage of the lake. Moreover, a significant increase in SWL was also reported in this region during the 2019–2020 interval for Lake Turkana (Salza, 2023; Zen et al., 2023); Lakes Albert, Rukwa, Kyoga, and Tanganyika (Papa et al., 2023); and Lake Victoria (Pavur and Lakshmi, 2023). The same increasing SWL trends were also recorded over the 2010–2020 period for the lakes of Kenya's Central Rift Valley (Lakes Baringo, Bogoria, Elementaita, Nakuru, Naivasha, and Solai), with peaks recorded in 2020 (Herrnegger et al., 2021; Muita et al., 2021). In most of these cases, precipitation was identified as the main factor driving ground and surface water variations. This finding supports the results of previous studies carried out in this region (Conway, 2002; Kimaru et al., 2019). In addition, Gbetkom et al. (2023), Mahamat Nour et al. (2021), Nicholson and Yin (2001), Scholz et al. (2011), and Stager et al. (1997) showed that SWL fluctuations in African lakes are associated with geological, climatic and other environmental factors. However, Ndichu et al. (2022) argued that climatic drivers should be coupled with astronomical influences to explain extreme climate events and SWL fluctuations in the East African region.

Floods or droughts in East African lakes are primarily major environmental and socioeconomic challenges in these subregions. For instance, within their different basins, Lake Victoria, Lake Tanganyika, and the two lakes Malawi and Malombe provide important ecosystem services to ~42, 13, and 10 million people, respectively (Awange et al., 2019; Makwinja et al., 2021). Lakes in this region also host important biodiversity (Darwall et al., 2005; Hongo and Mulaku, 2021; Odada et al., 2003; Stoyneva-Gärtner et al., 2020). For example, the rising level of Lake Victoria in 2020 led to the flooding of 8389 ha of land and 6399 ha of cropland in Kisumu County (Kenya), the inundation of the surrounding areas, the displacement of local populations, and the blackout of regional electricity in Uganda (GEOGLAM, 2020). In addition, other negative effects of rising lake levels in Kenya's Great Rift Valley for local communities include the flooding of hospitals, roads, homes, schools and other socioeconomic infrastructure, such as hotels and other tourist facilities (Herrnegger et al., 2021; Victor et al., 2023). Torrential rains and rising waters on Lake Tanganyika in 2021 affected approximately 281,180 people in the Tanganyika Province of the Democratic Republic of the Congo (DRC) (Unicef, 2021). On the Burundian side of the Lake Tanganyika basin, the rising waters of the lake have affected ~50,000 people and displaced more than 20,000 people in Gatumba and Rukaramu, where essential field crops have flooded. Additionally, the inhabitants, mostly farmers or fishers, have lost their yearly food stocks (IOM, 2021, 2020). In Burundi's Rumonge Province, 1666 people out of 2217 households affected by floods were displaced (OCHA, 2021).

Furthermore, in addition to flooding, the current and expected effects of climate change on the Lake Tanganyika watershed include increased air temperature and ET, food security due to declining crop yields, reduced water availability, and soil erosion (Ministry of Foreign Affairs of the Netherlands, 2018). Using a high-emission scenario (RCP 8.5) projected over the Lake Tanganyika basin, Sterckx et al. (2023) reported a surface water warming of 3 °C and increased stratification in the upper 150 m of the water column at the end of the century.

Therefore, the interactions of Lake Tanganyika and its watershed with climate change have already been well documented. However, much remains to be done to understand the watershed water balance at the monthly time scale. In addition, we explored the link between total water storage (TWS) variation at the basin scale with the SWL. We investigated the possibility of anticipating major variations in the SWL of Lake Tanganyika leading to flooding. Finally, we provide a description of how the lowlands surrounding the lake were exposed to flooding. Indeed, studying flood exposure is potentially vital, at least in terms of limiting loss of life and massive displacement during major floods and for other societal and disaster purposes in the region. Therefore, the aims of this study are to (1) analyze the variations in the water balance of Lake Tanganyika under recent climatic conditions (2003–2021), (2) map the risk of ex-

posure to flooding on the northern shores of the lake (among the most urbanized shores), and (3) explore early warning flood indicators. To this end, remote sensing or/and reanalysis data of rainfall, E and ET, soil moisture, and TWS were combined with the Lake Water Level (LWL) database (derived from altimetry measurements) to correlate the spatiotemporal dynamics of climate variables in the watershed with changes in the lake water balance. Sentinel–2 data are used to map flooding on the shores of Lake Tanganyika.

In Section 2, bellow, we describe the data used and methodology adopted to perform our main objective; in Section 3, the major results obtained are analyzed; and in Section 4, before the conclusion, we discuss the implications, limits, and perspectives for this research.

2. Study area, datasets and methodology

2.1. The study region

Lake Tanganyika is located in the western branch of the East African Rift Valley (Fig. 1). This lake is documented as the longest (673 km) and second deepest (1470 m) freshwater lake in the world, with an average depth of 570 m, an average width of 50 km and a surface area of 32,900 km^2 (Ivory et al., 2021; Verburga and Hecky, 2009). It is the largest freshwater reservoir in Africa, at 18,900 km^3 (Ivory and Russell, 2016; Sterckx et al., 2023), and contains 17% of the free freshwater on the Earth's surface (Plisnier et al., 2018). The Lake Tanganyika watershed covers an area of more than 220,000 km^2 (Fig. 1). The watershed's climate is divided between the dry season (June to September or October) and the rainy season (October or November to May of the following year) (Niyoyitungiye, 2019). The onset, duration and intensity of the rainy season are governed by the north–south shift in the intertropical convergence zone (ITCZ) associated with the El Niño–Southern Oscillation (ENSO) (Sterckx et al., 2023). Warm ENSO events lead to increased rainfall in East Africa, while colder ENSO events result in below-average rainfall (Conway, 2002). Thus, from north to south, rainfall shows a gradient in terms of amount and timing across the watershed, with ~1600 mm/year recorded in the north and ~870 mm/year in the south (Ivory et al., 2021). The temperature depends on the altitude and varies during the year between 22.8 and 24.8 °C at 900 m of altitude and between 15.8 and 20.4 °C at 1500 m of altitude (Ivory and Russell, 2016).

2.2. Data description

2.2.1. The HYDROWEB water level data

The Hydroweb database (https://hydroweb.theia-land.fr/) was used to obtain Lake Tanganyika surface water storage (SWS) fluctuations. This database contains and delivers the time series of water levels of great lakes, reservoirs, and rivers produced by LEGOS (Laboratoire d'Etudes en Géophysique et Océanographie Spatiales) and CLS (Collecte Localisation par Satellite) (Crétaux et al., 2011).

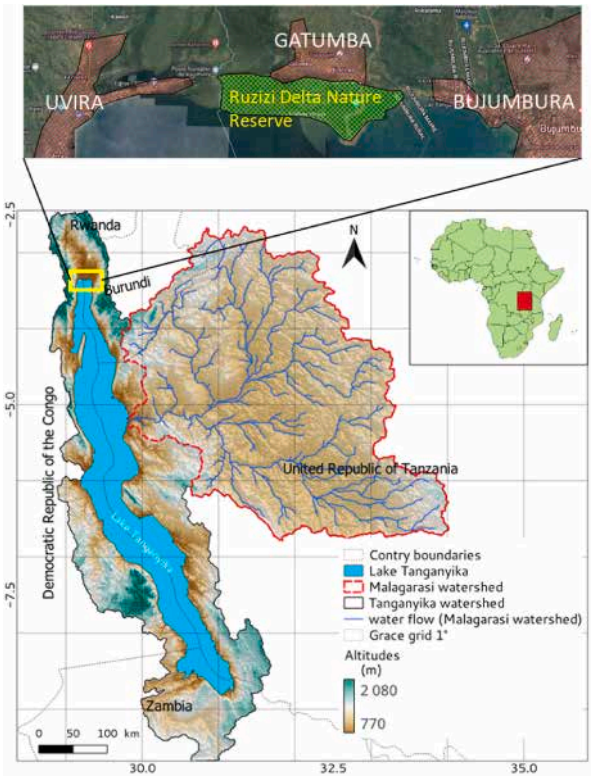

Fig. 1. The Lake Tanganyika watershed location (country borders are outlined in black, and the Malagarasi watershed is delineated in red). In the yellow box, the most urbanized northern shores of the lake are within the city of Uvira in the DRC (to the west) and Bujumbura, Gatumba, and the Ruzizi Delta Nature Reserve in Burundi (to the center and the east). (For interpretation of the references to color in this figure legend, the reader is referred to the Web version of this article.)

Times series are obtained after corrections (geophysical, environmental, and instrumental) of the altimetry measurements recorded by radar sensors (Topex/Poseidon, ERS-2, GFO, Jason-1, Envisat, Jason-2, Jason-3, CryoSat-2, Saral/Altika, Sentinelle-3A and Sentinelle-3B satellites) (Crétaux and Birkett, 2006). The orbital cycles of each mission vary from 10 to 35 days and drive the timporal resolution of the measurements over a given lake or river (Crétaux and Birkett, 2006). Using the SWL variations since 1992 over Lake Tanganyika and its average water extent allows us to determine the SWS fluctuations over the period of study (2003–2021) (Crétaux et al., 2016). The accuracy of altimetry over such large lakes is assumed to be subdecimeter according to several studies that aimed to evaluate the performances of satellite altimetry over lakes (Nielsen et al., 2015; Ričko et al., 2012; Vuglinsky et al., 2023). More details on the error budget of satellite altimetry and the different sources of uncertainties, namely, tropospheric and ionospheric correction, tracking and retracking systems, mode of range measurements, low-resolution mode (LRM) and synthetic radar aperture (SAR), are given in Crétaux et al. (2009) and Taburet et al. (2020).

2.2.2. Rainfall products

We used various rainfall products to calculate the generic water balance equation and quantify flow variations in the lake from flow variations in the rest of the basin. Since precipitation datasets may present differences depending on the studied region, the aim is to identify the most appropriate rainfall dataset for our study location. We selected 5 precipitation datasets that are used in the current literature to understand the role of precipitation in the water balance of the Tanganyika basin.

2.2.2.1. Integrated Multi-satellitE retrievals for the GPM (global precipitation measurement) (IMERG). These data are satellite-based gridded datasets of rainfall amounts at half-hourly time intervals with a spatial resolution of 0.1° × 0.1°, and temporal coverage starting at 2000-06-01 over the majority of the Earth's surface (Tan et al., 2019). IMERG combines passive-microwave (PMW) sensors from the entire GPM constellation (more than 10 satellites) and infrared (IR) sensors from geostationary satellites. All satellite microwave precipitation estimates are intercalibrated, merged, and interpolated with microwave-calibrated infrared (IR) satellite estimates and precipitation gauge analyses. IMERG products available on the National Aeronautics and Space Administration (NASA) website (https://gpm.nasa.gov/data) are organized into IMERG-E (Early), IMERG-L (Late) and IMERG-F (Final). The early and late products are generated in near real time with 4 h and 12 h time lag respectively, and the final product takes two months. For this study, we worked with the most recent product (version 6) of the IMERG-F product, as it is calibrated with ground rainfall stations to increase accuracy (Ma et al., 2020). Daily data from 2003-01-01 to 2021-09-30 were downloaded and subsequently summed across the Lake Tanganyika watershed at the monthly timescale.

2.2.2.2. Global satellite mapping for precipitation (GSMAP). As for IMERG, this rainfall product combines multi-satellites data from the PMW and IR images. The Japan Aerospace Exploration Agency (JAXA) implemented this project in 2002, using a constellation of 20 satellites covering the globe between latitudes 60°S and 60°N (Ramadhan et al., 2023). The products are regularly gridded rain rates with a spatial resolution of 0.1° × 0.1° generated by the following main steps: (a) retrieval of the precipitation rate from passive microwave data using a Kalman filter approach, (b) propagation of the estimated precipitation rates using a backward- and forward-morphing technique, and (c) refinement of precipitation data based on the brightness temperature and surface precipitation rates (Peña-Guerrero et al., 2022). GSMap data are divided into GSMaP_Now (real-time with 0 h latency), GSMaP_NRT (near-real-time with 4 h Latency), and GSMaP_MVK (post-real-time with 3-day latency) datasets (Priyambodoho et al., 2021). Daily GSMaP_MVK data from 2003 to 2021 were downloaded from https://sharaku.eorc.jaxa.jp/GSMaP/ and accumulated over the Lake Tanganyika watershed on a monthly timescale.

2.2.2.3. Multi-source weighted-ensemble precipitation (MSWEP). MWSEP data provide a global rainfall estimation at a temporal resolution of 3 h and a spatial resolution of 0.1° (Peña-Guerrero et al., 2022). The products include four satellite precipitation products (TMPA 3B42RT, CMORPH, global satellite mapping of precipitation and gridded satellite (GridSat), Global Satellite Mapping of Precipitation (GSMaP)), two reanalysis precipitation datasets (ECMWF interim reanalysis and JRA-55), and observations from ~75,000 rain gauges worldwide (Li et al., 2022). The MWSEP data merging process includes the evaluation and validation of source data, the weight calculation and integration of satellite and reanalysis precipitation data, and finally bias correction of the merged data (Beck et al., 2019). The second version of the MSWEP (MSWEP v2), available at the official website https://www.gloh2o.org/mswep/ was downloaded from 2003 to 2021 and accumulated over the Lake Tanganyika watershed on a monthly timescale.

2.2.2.4. Climate Hazards Group infrared precipitation with station data (CHIRPS). CHIRPS images display daily, monthly, pentadal, and decadal rainfall histories from 1981 to the present day at a spatial resolution of 0.05° and global coverage within 50° north and south latitudes and 180° west and east longitudes (Sacré Regis M. et al., 2020). The U.S. Geological Survey (USGS) and the Climate Hazards Group at the University of California, Santa Barbara, and observations from the Climate Prediction Center and the National Climatic Data Center were involved in developing the CHIRPS dataset (Ocampo-Marulanda et al., 2022). The CHIRPS data include quasiglobal geostationary thermal infrared satellite observations, monthly rainfall climatology CHPClim (Climate Hazards Group Precipitation Climatology), Tropical Rainfall Measuring Mission (TRMM) 3B42 data, atmospheric model rainfall fields from NOAA CFS (Climate Forecast System), and rainfall observations from different sources, including national or regional meteorological services (Funk et al., 2015). The second version of the monthly CHIRPS data was downloaded at https://data.chc.ucsb.edu/products/CHIRPS-2.0/ for the period 2003–2021.

2.2.2.5. ERA5-land (total precipitation). Within the Copernicus Climate Change Service (C3S), the European Centre for Medium-Range Weather Forecasts (ECMWF) produces the ERA5 (ECMWF Reanalysis v5) reanalysis, which provides a detailed record of the global atmosphere, land surface and ocean waves from 1950 onward (Hersbach et al., 2020). This ERA5 product, with a spatial res-

olution of 0.25°, is the ECMWF's fifth-generation reanalysis of global climate and weather (Muñoz-Sabater et al., 2021). The reanalyzed products combine several observations of wind, pressure, temperature, precipitation and humidity from several satellites and observations near the Earth's surface and over the oceans, upper air soundings and atmospheric measurements using aircraft instruments (Bathelemy et al., 2022). ERA5 is based on the Integrated Forecasting System (IFS) Cy41r2 and features year-round hourly outputs (Hersbach et al., 2020). ERA5-Land produced at a higher spatial resolution of 0.1° is a rerun of the land component of the ERA5 reanalysis dataset achieved by implementing a series of improvements over ERA5 to make it more accurate for all types of land applications (Pelosi et al., 2020). Therefore, ERA5-Land has good applicability for land surface processing, and total rainfall data (monthly averaged reanalysis) were downloaded for the 2003–2021 period at https://cds.climate.copernicus.eu/cdsapp#!/dataset/reanalysis-era5-land-monthly-means?tab=overview.

2.2.3. ET and E products

To identify the most appropriate ET and E products for our study area, we used two types of products for each variable (ET and E) when calculating the generic water balance equation. These two products, covering the period 2003–2021, are freely available.

2.2.3.1. ERA5-land (total evaporation). Monthly averages of total evaporation reanalysis data at a 0.1° spatial resolution for the period 2003–2021 were also downloaded from the above ECMWF website (ERA5-Land). As the total evaporation of ERA-Land includes a simplified representation of vegetation transpiration (Fedotova and Gosteva, 2021; Zsoter et al., 2020), this product was used in this study to estimate E from Lake Tanganyika and ET on watershed land.

2.2.3.2. MODIS product. The other dataset used in this study to analyze land ET in the Lake Tanganyika watershed is Version 16A2 of the Moderate Resolution Imaging Spectroradiometer (MODIS), also known as MOD16A2. This product estimates terrestrial ET as the sum of soil and canopy E and transpiration from plant leaves and stems (Mu et al., 2011). The MOD16A2 product estimates ET based on the Penman–Monteith equation, with the main inputs including global daily meteorological data, surface albedo, land cover classification and remotely sensed vegetation properties such as the leaf area index/fraction of absorbed photosynthetically active radiation (LAI/FPAR) (Degano et al., 2021). All the data are produced worldwide with a spatial resolution of 500 m and correspond to the pixels least affected by clouds and other deformations over an 8-day observation period (Che et al., 2022). The MOD16A2.006 (MOD-16A2 Collection 6) dataset for the period 2003–2021 was downloaded from the USGS website https://lpdaac.usgs.gov/products/mod16a2v006/.

2.2.3.3. GLEV. Monthly changes in Lake Tanganyika E volume from 2003 to 2018 were analyzed through Global Lake Evaporation Volume (GLEV) datasets. GLEV products are derived from satellite observations and modeling tools by Zhao et al. (2022) to quantify the E volume of 1.42 million global lakes from January 1985 to December 2018. For a given lake, the GLEV provides monthly E volume time series data obtained by pairing monthly lake surface area measurements from the Landsat-based global surface water dataset (GSWD) with monthly meteorological data (TerraClimate, ERA5, and the Global Land Data Assimilation System (GLDAS)). For each lake, the E volume is derived as a function of the E rate for each month, the monthly surface area, and the percentage of time per month when a lake is fully covered by ice (Zhao et al., 2022). We used GLEV products in this study because the data are freely available at https://zeternity.users.earthengine.app/view/glev.

2.2.4. Soil moisture data (GLDAS-CLSM)

The Global Land Data Assimilation System (GLDAS) uses ground observation and satellite data as inputs in advanced land surface modeling and data assimilation techniques to generate variables associated with the hydrological components on continents (Rodell et al., 2004). The GLDAS database contains four land surface models (LSMs): the Noah model, the catchment land surface model (CLSM), the community land model (CLM), and the variable infiltration capacity (VIC) (Kumar et al., 2006). GLDAS provides global land surface information such as soil temperature, evaporation, surface soil moisture, and root-zone soil moisture (RZSM) data at 1° and 0.25° spatial resolutions; 3-hourly, daily, and monthly temporal resolutions; and a period of simulation starting in 1948. This study used the GLDAS-CLSM product version 2.2, which simulates RZSM (0–100 cm) at a spatiotemporal resolution of 0.25° daily. The data covering the period from 2003 to 2021 are available on the NASA website at https://disc.gsfc.nasa.gov/datasets?keywords=GLDAS.

2.2.5. GRACE products

The Gravity Recovery and Climate Experiment (GRACE) mission, launched in 2002, allowed continuous monitoring of ocean mass change between 2002 and 2017 (Tapley et al., 2004). GRACE was decommissioned in 2017, and its successor, GRACE Follow-On (GRACE-FO), was launched in May 2018 (Landerer et al., 2020). In this study, we used products from GRACE and GRACE-FO for monthly TWS monitoring in the Lake Tanganyika watershed from 2003 to 2021. These GRACE missions map monthly variations in the Earth's gravity field, with a spatial resolution of approximately 300 km (Tapley et al., 2004). Monthly variations are corrected for the solid Earth changes that affect gravity fields and are not related to the redistribution of water within the Earth's fluid envelope. It allows us to estimate the sum of all water mass variations at the continental surface and in the soil, including snow water equivalent, surface runoff, soil moisture and groundwater storage (Famiglietti et al., 2011; Tapley et al., 2019). In this study, we considered the GRACE CNES L4 ensemble V1.5.3 (http://ftp.legos.obs-mip.fr/pub/soa/gravimetrie/grace_legos/V1.5.3), which was updated from Blazquez et al. (2018). This GRACE product has a monthly temporal resolution and a spatial resolution of 1°, which provides maps of the accumulation of all forms of water stored above and below the Earth's surface worldwide.

2.2.6. Sentinel–2 data

Sentinel–2 data were used to map submerged areas on the northern shores of Lake Tanganyika. The European Space Agency (ESA) launched the Sentinel–2 (A and B) satellite in June 2015, and the data which were collected at high spatial resolutions of spectral bands ranging from 10 m to 60 m, have a global fine revisit frequency of 5 days (Gatti and Bertolini, 2015). The multi-spectral instrument (MSI) sensors onboard Sentinel–2 satellites collect images with 13 spectral bands in the visible/near-infrared (VNIR) and shortwave infrared (SWIR) spectra (Yu et al., 2020). In this study, we used the Sentinel–2 MSI Level-1C product hosted on the Google Earth Engine (GEE) platform (https://developers.google.com/earth-engine/datasets/catalog/sentinel-2). For each satellite image, only band3 (or Green, with a wavelength of 0.537–0.582 at a spatial resolution of 10 m) and band11 (or SWIR1, with a wavelength of 1.539–1.681 at a spatial resolution of 20 m) were exploited.

2.2.7. The FABDEM product for the digital elevation model (DEM)

We used the Forest And Buildings removed Copernicus DEM (FABDEM) data to determine the surface land elevations in the Lake Tanganyika watershed (Fig. 1). These data are a global DEM map obtained after correcting artifacts from forests and buildings removed from the Copernicus digital elevation model using random forest machine learning models (Hawker et al., 2022). These data are produced at a spatial resolution of 30 m (Marsh et al., 2023) and are available at the following address https://www.fathom.global/product/fabdem/.

2.2.8. Discharges of the malagarasi, Ruzizi and Lukuga Rivers

To compensate for the lack of in situ discharge records for the Malagarasi, Ruzizi and Lukuga Rivers during the study period, we calculated the average daily discharge (m/s) from 2003 to 2020 using the MGB-IPH hydrological model. The MGB-IPH is a large-scale hydrological model distributed in square grid cells that represent hydrological processes in large-scale watersheds, such as flow propagation through the river network (Allasia et al., 2006). More descriptions of the MGB-IPH hydrological model are provided in Collischonn et al. (2007). The data are provided 10 m after the lake outlet (for Lukuga, which exits the basin) and 10 m before the lake (for Malagarasi and Ruzizi, which flow into the lake). The dataset is available at Hydrological Reanalysis for the Congo River Basin (1983–2020) (zenodo.org) (see Wongchuig et al., 2023 for more details). These data were used to compute the basin water balance.

2.3. Methodology

2.3.1. Lake Tanganyika watershed water balance computation and water storage monitoring

A spatial mask using the Tanganyika basin limits was applied to the GRACE data to extract the raw GRACE satellite TWS values within our area of interest. Pixels fully included in the boundaries were retained, and for partially included pixels, we weighted the TWS by the fraction of the pixel within the basin (see Fig. 1 for the spatial distribution of the Grace grid in the study area). The raw TWS values from the GRACE satellite already represent the total monthly variations in water at the watershed surface and can be expressed as the equivalent water height (EWH) in km^3. However, in this study, we harmonized the raw variations in TWS (ΔTWS) with those in SWS and other water inflows over the 2003–2021 period, using January 2003 as the starting date, as follows:

$$\text{at } i = 1 \rightarrow n\text{: } \Delta TWS_{(i)} = TWS_{(i)} - TWS_{(0)} \quad (1)$$

where $TWS_{(i)}$ is the monthly GRACE-based raw EWH value over the entire watershed at *i*. $\Delta TWS_{(i)}$ is expressed in km^3 and computed for the 2003–2021 period.

The obtained ΔTWS over the entire watershed allowed us to determine the water balance for the watershed and to monitor water volume changes in the main reservoirs. Indeed, for a given period in a closed system, ΔTWS can be equated to the difference between the total water received and lost (Biancamaria et al., 2019; Hu et al., 2021) or can be analyzed as the total variation in water volume in the various reservoirs of the watershed (Pham-Duc et al., 2020). The first approach is analyzed in this study using Equation (2) below, and the second method is implemented with Equation (3). All the results in Equations (2) and (3) are expressed in km^3.

2.3.1.1. Calculate the variations in water input and output in the watershed. The main objective here is to identify the precipitation, E and ET datasets best suited to our case study and to compute the water balance of the Lake Tanganyika watershed. To this end, the ΔTWS was compared to the generic water balance equation for a watershed based on Equation (2) below (see Section 1 of the Supplementary Material for more details on how we integrated this equation for this study). We applied this equation for all possible combinations of precipitation, E and ET datasets used in this study.

$$\text{at } i = 1 \rightarrow n\text{: } \Delta TWS_{(i)} = P_{(i)} - ETR_{(i)} - Q_{(i)} \quad (2)$$

where P is the precipitation, ETR is the sum of the E and ET, and Q is the water discharge at the outlet of the basin.

Spatial masks were applied to the P data (IMERG, GSMAP, ERA5, CHIRPS, and MSWEP), as well as the ETR data (GLEV, MODIS, and ERA5), to extract these values within our area of interest.

2.3.1.2. Water volume variations in the watershed's water reservoirs. According to Nigatu et al. (2021), Pham-Duc et al. (2020), Springer et al. (2023), Xiang et al. (2016), and Zhang et al. (2017), the ΔTWS integrates changes in all water stored above and below the Earth's surface (on a regional or global scale). ΔTWS corresponds to the sum of the water volume variations stored in four different reservoirs: surface water storage (in rivers, lakes and wetlands; ΔSWS), RZSM storage (ΔSMS), ice and snow storage (ΔISS), and groundwater storage (ΔGWS). ΔISS has been neglected for the Lake Tanganyika watershed. TWS and SMS were com-

puted from GRACE and GLDAS-CLSM images, respectively (described in subsections 2.2.5 and 2.2.4, respectively), and SWS was deduced from HYDROWEB water level data (described in subsection 2.2.1). The ΔGWS is unknown and can therefore be derived from ΔTWS, ΔSWS and ΔSMS using Equation (3) as the difference between ΔTWS and the sum of ΔSWS and ΔSMS. Calculating the ΔGWS allows us to determine the proportion of water contained in each reservoir at the watershed scale and to deduce the percentage variations in water volume per reservoir (see Section 2 of the Supplementary Material for more details on ΔSWS, ΔSMS and ΔGWS computing).

$$\text{at } i = 1 \rightarrow n\text{: } \Delta TWS_{(i)} = \Delta SWS_{(i)} + \Delta SMS_{(i)} + \Delta GWS_{(i)} \quad (3)$$

where $\Delta TWS_{(i)}$ is the TWS variation at *i*.

2.3.2. Spatial and temporal analyses of key climate variables in the Lake Tanganyika watershed

With respect to Equation (2), time series of rainfall and E/ET were calculated for the lake and the whole watershed, to analyze the spatial and temporal variability in these climatic variables at the watershed scale and their influence on the water balance of Lake Tanganyika.

These time series give an average monthly value per date for the lake or watershed land (for the period 2003–2021). Each time series of the original signal is then decomposed into three independent components using the Hanning filter (Hattermann et al., 2021): i) the trend signal representing the interannual variability, ii) the seasonal signal and iii) a residual component. Rainfall and E trends on the lake and over the watershed land can then be analyzed.

In addition, for the selected rainfall data, the time series of monthly rainfall images for the entire watershed were decomposed into trend, seasonal and residual signals. We then applied multivariate statistical analysis using empirical orthogonal function (EOF) to trend and seasonal signals to highlight the spatial variability in rainfall for the period 2003–2021. The EOF method is very useful for identifying coherent spatial and temporal variability when processing a large multispectral or time series dataset (Li et al., 2013). We used this method to reduce the redundancy in each decomposed signal and merge the coherent variations in the initial information into a small number of new components (independent variables) that were statistically uncorrelated. These new components project the initial information into an orthogonal basis. This method is ideally suited to the spatial and temporal analysis of seasonal signal and trend images, given the large number of images used to cover the period 2003–2021. The results highlight trends and seasonal spatial patterns in rainfall across the watershed using eigenvectors (Li et al., 2013; Toumazou and Crétaux, 2001) and their evolution over time using eigenvalues.

2.3.3. Flood mapping on lake shores and nearby lowland areas

a. Submerged soil mapping.

It is essential to map the distribution of soils that have been submerged due to the observed variations in lake water level caused by the dynamics of climatic variables in the watershed. This allows us to study the vulnerability of lake shores and nearby lowland areas to observed SWS variations. The MNDWI spectral water index (Xu, 2006) offers this possibility, using the formula below, to distinguish water surfaces from the rest of the land cover on a satellite image (Herndon et al., 2020). The Sentinel–2 images acquired between 2017 and 2022 were corrected from level 1C to level 2A (atmospheric correction) and used for this mapping.

$$MNDWI = (\rho\text{Green} - \rho\text{SWIR1})/(\rho\text{Green} + \rho\text{SWIR1}) \quad (4)$$

where ρ Green is the green spectral band and ρ SWIR1 is the SWIR1 spectral band.

The obtained MNDWI values ranged from −1 (remaining land cover) to 1 (water surface). Each MNDWI image was then thresholded at 0.05 (Xu, 2006) and multiplied by the spatial resolution of Sentinel–2 (20 m) to obtain water body and submerged soil areas (Deus and Gloaguen, 2013).

3. Results

3.1. Lake Tanganyika basin water dynamics and climate variations

3.1.1. The basin's water budget

Fig. 2 illustrates the water balances obtained by combining precipitation data (PEra, PChirps, PGsmap, PImerg, and PMswep) with E and ET data (EMod, and EEra). For example, PEra_EEra is the combination of the ERA5 total precipitation and the ERA5 total evaporation. Each water balance is overlaid with the ΔTWS to identify the sets of precipitation, E and ET data that are able to close the Lake Tanganyika basin water budget.

The PEra_EMod balance best matches the ΔTWS. The seasonality of these two curves is well synchronized, and their time series describe the same interannual dynamics, showing a reduction in the total volume of water in the basin between 2003 and 2006 and a progressive increase from 2007 onward. This balance is the one with the smallest deviation from ΔTWS ~25 km^3 (see Section 3 of the Supplementary Material). For the PImerg_EMod balance, the variations are similar to those of the ΔTWS until 2009 (decrease between 2003 and 2006 and then increase beginning in 2007) but progressively decrease beginning in 2010 and remain lower than the ΔTWS until 2018. The difference between these two balance calculations is found in the measurement of *Δ_ld_flow*. The three other combinations with EMod show that *Δ_lk_flow* and *Δ_ld_flow* are always lower than 0, with water balances consequently always being lower than TWS. An underestimation of precipitation from the corresponding datasets presumably explains these observations (the water losses for *Δ_lk_flow* up to −200 km^3, particularly for PChirps_EMod and PMswep_EMod).

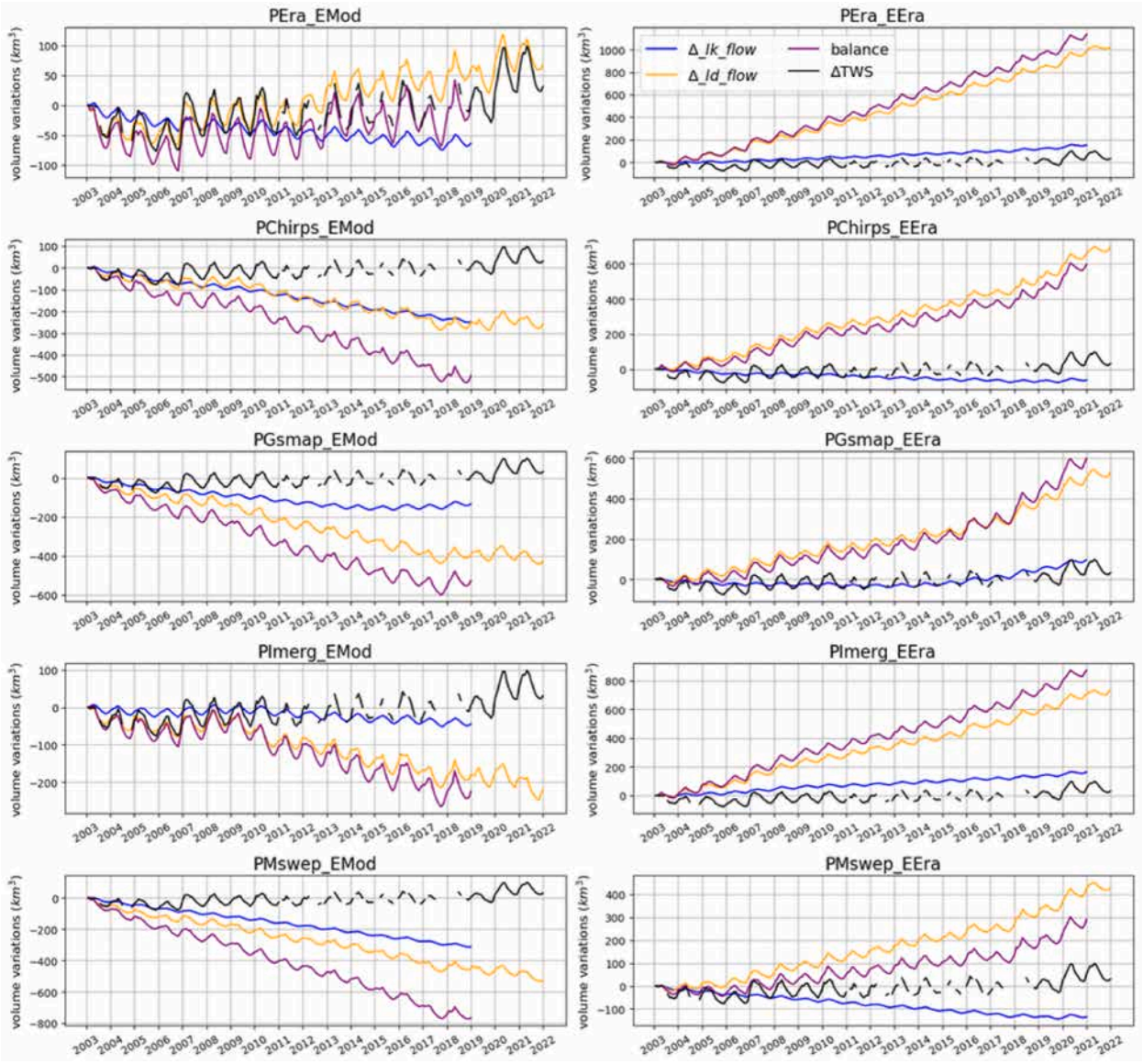

Fig. 2. The water balance of the Lake Tanganyika basin was calculated with different datasets. In the left column, the combinations of precipitation with EMod (GLEV E + Modis ET) are shown; in the right column, the combinations with EEra (ERA5 total evaporation) are shown. Each plot shows the volume of *Δ_lk_flow* (for lake, blue), *Δ_ld_flow* (for land, yellow), water balance (purple), and Δ_TWS (black). Since the GLEV E time series ends in 2018, all combinations with EMod ended in 2018. (For interpretation of the references to color in this figure legend, the reader is referred to the Web version of this article.)

None of the balances obtained with EEra match the ΔTWS. The water balances are always greater than the ΔTWS. The PEra_EEra and PImerg_EEra balances can be explained by an underestimation of E and ET by ERA5. This underestimation combines with that of precipitation to explain the PChirps_EEra, PGsmap_EEra, and PMswep_EEra balances.

The above results show that the accumulation of *Δ_lk_flow* and *Δ_ld_flow* volumes lead to an accumulation of error amplitudes due to the underestimation of precipitation, E and ET values and leads, for most combinations, to an incorrect evaluation of the water balance. Ultimately, only the combination of PEra with EMod is strongly correlated with the TWS observed using the GRACE gravity dataset and therefore allows closing the water balance.

The uncertainty in the ΔTWS was quantified using 216 GRACE solutions and described for each month as the relative bias between the standard deviation and mean values. The result is an uncertainty mean value of 5.22 km^3/month (Fig. 1s, in Section 6 in the Supplementary Material).

The uncertainty in the water budget estimate propagated from that in the rainfall, evaporation and evapotranspiration. For the rainfall variable, the uncertainty was estimated at 13 mm/month using the mean and standard deviation of the 5 time series of total monthly precipitation (IMERG, GSMAP, MSWEP, CHIRPS and ERA5-Land) (see Section 5 in the Supplementary Material). This value summarizes the difference in the accumulated precipitation among all the products considered in this study, which can be attributed

to an overall uncertainty if we consider the combination of them. Concerning E and ET, Zhao et al. (2022) published an uncertainty of ~9.93% for GLEV products, and Yu et al. (2023) found an uncertainties of ~9 mm/month and ~12 mm/month for the MOD16A2 and ERA5 products, respectively, under extreme conditions over the United States.

3.1.1.1. Comparing the TWS derivative with the total water flux variations in the watershed. To analyze the discrepancies observed in the obtained water balances without the effects of the cumulative amplitude error, we compared the derivative of TWS (*d*TWS) with the monthly difference between total water received and total water lost (P_{basin} - E_{basin}) in the watershed (see Section 4 in the Supplementary Material for more details on how we computed *d*TWS and [P_{basin} - E_{basin}]).

The *d*TWS curve has an amplitude of 60 km³, with two peaks recorded in 2006–2007 (> 43.7 km³) and 2009–2010 (> 28.7 km³). Minima are approximately −20 km³, and the maxima are more variable.

For the EMod combinations, the minima are consistent with those of *d*TWS (~-20 km³). PEra_EMod and PImerg_EMod are the only ones where the variations in maxima have nearly the same values as *d*TWS, but the PEra_EMod curve is the one that most accurately estimates the 2006–2007 (~40 km³) and 2009-10 (> 20 km³) peaks (Fig. 3). On the three other curves of the EMod combinations, the maxima of the two peaks are regularly lower than those of *d*TWS.

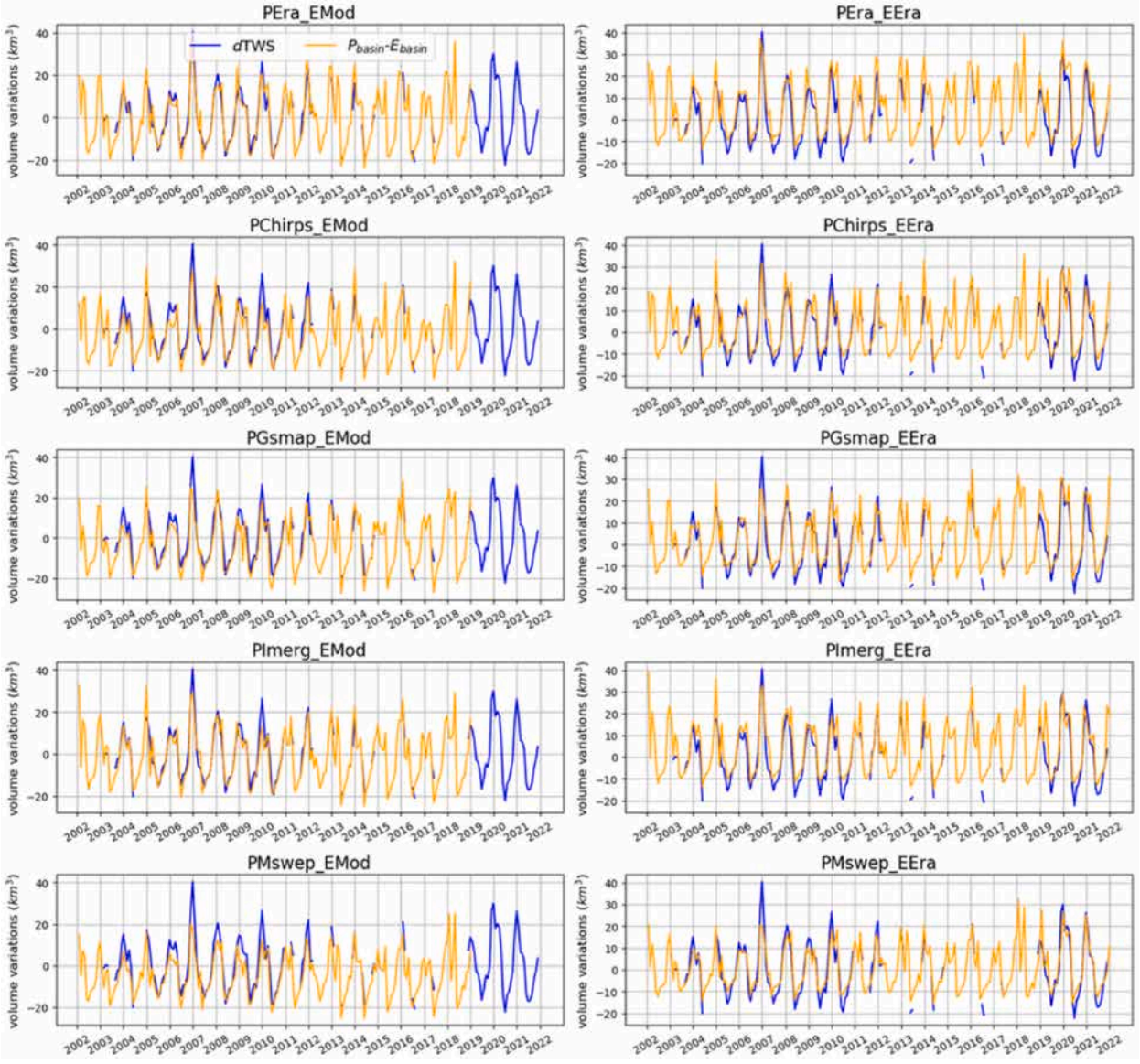

Fig. 3. Variations in *d*TWS (blue) and [P_{basin} - E_{basin}] (orange). In the left column are the combinations of precipitation with EMod (GLEV E + Modis ET), and in the right column, the combinations with EEra (total evaporation from ERA5) are shown. Since the GLEV E time series ended in 2018, the combinations with EMod ended in 2018. (For interpretation of the references to color in this figure legend, the reader is referred to the Web version of this article.)

For the combinations with EEra, the minima vary around −10 km^3. This confirms the low estimates of E and ET by ERA5 and justifies once again the Δ_lk_flow, and Δ_ld_flow volumes obtained for the water balances with EEra (Fig. 2). The variations in the maxima are better estimated by comparison with the combinations with EMod, but the values of the maxima of both peaks (2006–2007 and 2009–2010) remain consistently lower than those of dTWS.

These results show that the water budget is therefore only possible when precipitation inputs are balanced with E and ET losses even during anomalies (2006–2007 and 2009–2010), as is the case for the PEra_EMod balance.

3.1.1.2. The spatial distribution of rainfall per dataset. A further explanation of the discrepancies observed in the water balances is highlighted by analyzing the spatial distribution of precipitation per dataset, according to the topography of the Lake Tanganyika watershed. For each dataset, an average image of rainfall estimation over the entire basin for the observed period was computed using 6940 daily images between January 2003 and December 2021 (Fig. 4).

We used the FABDEM described above (Section 2.2.7) to distribute the rainfall across the total watershed of Lake Tanganyika considering its topography, which is characterized by three distinct main entities (Fig. 1): the lake (~770 m, dashed black in Fig. 4b–f), the Malagarasi basin (between ~770 m and <1400 m, dashed red in Fig. 4b–f) and the mountains around the lake in the rest of the watershed (>1400 m). The average rainfall in the Malagarasi basin is homogeneous and constant at approximately 120 mm/day for all the rainfall datasets. However, ERA5 and IMERG stand out because of their estimation of rainfall in the lake of ~200 mm/day, and only ERA5 shows rainfall average > 320 mm in the mountains. In the vicinity of the lake, all the other datasets showed rainfall deficits, which likely explains why only ERA5 was able to close the watershed's water budget, as shown in Fig. 2.

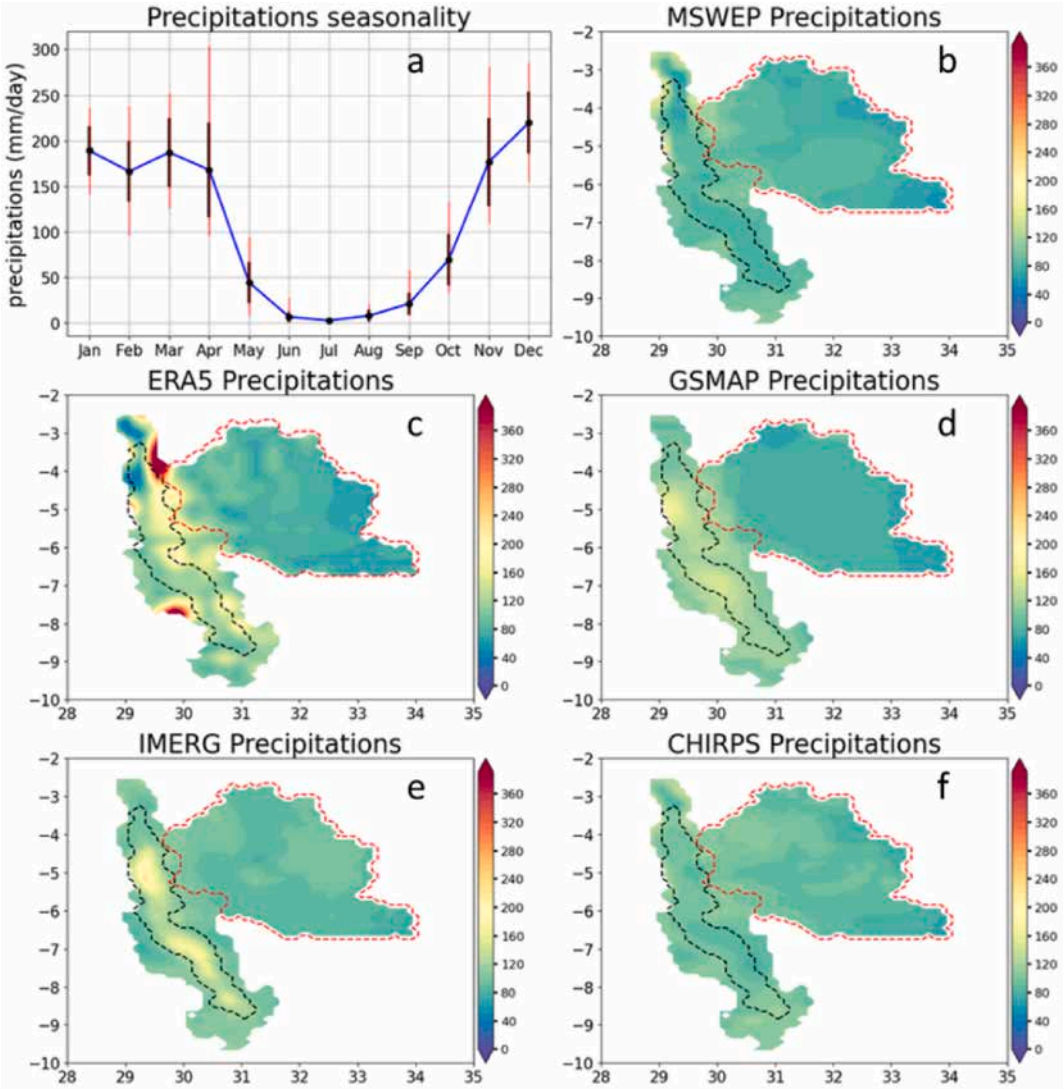

Fig. 4. Daily rainfall means (in mm/day, computed with the PEra dataset) in the Lake Tanganyika watershed (Fig. 4a) and map of the interannual daily mean precipitation (in mm/day) for each dataset.

These differences show that the ERA5 data, which were generated from a model that accounts for the topography and movement of cloud masses, are better suited to mountain areas than are the other observational data.

3.1.2. The basin's water storage components

To estimate the water quantities in each storage, we divided ΔGWS, ΔSWS and ΔSMS by ΔTWS. Over the observed period, the ΔTWS was composed of 57.7% of the ΔGWS, 41.8% of the ΔSWS, while the contribution of ΔSMS was less than 0.5% (Fig. 5). During the decreasing period, the ΔGWS represented ~83% of the ΔTWS in 2003 and ~60-50% between 2004 and 2006, while the ΔSWS varied between ~40 and 49%, except in 2003 (~17%). In 2020 and 2021 (at the end of the increase period), the ΔSWS corresponded to ~59% and ~80% of the ΔTWS respectively, and the ΔGWS was ~40% and ~19% of the ΔTWS respectively (Fig. 2s of Section 7 in the Supplementary Material). This means that during the observed period, water losses in the watershed, mainly within the decreasing period were greater through the groundwater, and recharging was provided by surface water.

The seasonality of ΔTWS and that of ΔGWS plot in the same pattern, with maxima observed in April and minima in September/October. The ΔSWS climatology is shifted by one month compared to those of ΔTWS and ΔGWS (maximum in May and minimum in November). For ΔSMS, maximum values are recorded in December. This seasonality showed that water recharge in the basin occurred mainly between October and April. The rainfall data plot in the same way, revealing that precipitation is the main source of water in the watershed.

ΔTWS was 89% correlated with ΔSWS and 90% correlated with the water balance obtained with PEra_EMod (Fig. 5). In the following subsection, we explain in greater depth the observed seasonality and trends in water storage components in the watershed.

For uncertainties in the data used, the value of 0.046 m^3/m^3 published by Liu et al. (2023) was considered for ΔSMS, and concerning ΔSWS, we calculated an average uncertainty of 5.9 km^3/month (see Sections 5 and 6 in the Supplementary Material).

3.1.3. Spatiotemporal dynamics of key climate variables in the watershed

We analyzed the space–time changes in the main climatic variables used for computing the water balance (precipitation, E and ET) to deduce their influences on the different volume variations (TWS, SWS, GWS, and balance) obtained in the watershed.

3.1.3.1. Lake trends compared with those in the rest of the watershed. Fig. 6 shows that in the lake, the general trend in rainfall increased (from 2003 to 2021) and that in the E was generally stable (from 2003 to 2018). However, until at least 2018, the E values remained consistently higher than the rainfall values despite their increase. This explains the regression of *Δ_lk_flow* on the PEra_EMod balance (Fig. 2). In the rest of the watershed, the overall trends in rainfall and ET from 2003 to 2021 are similar and positive and show that increases in precipitation are associated with increases in ET. However, from 2003 to 2005, ET values are on average higher than precipitation values, and the trends of both curves are slightly regressive. Water inputs by precipitation are then lower than losses by ET, which is why, on the PEra_EMod balance, *Δ_ld_flow* decreased over this period (Fig. 2). This ratio reverses beginning in 2006, and the *Δ_ld_flow* of the PEra_EMod balance increases again until 2021.

3.1.3.2. Trends and seasonality of total rainfall over the entire basin. The first mode of the interannual signal of total rainfall in the watershed (Fig. 7) explained 73% of these interannual dynamics and spatialized the observed increasing trend in rainfall. This trend was general for the entire watershed since the variances in EOF1 of this signal were all positive. The time series reported by PC1 was more

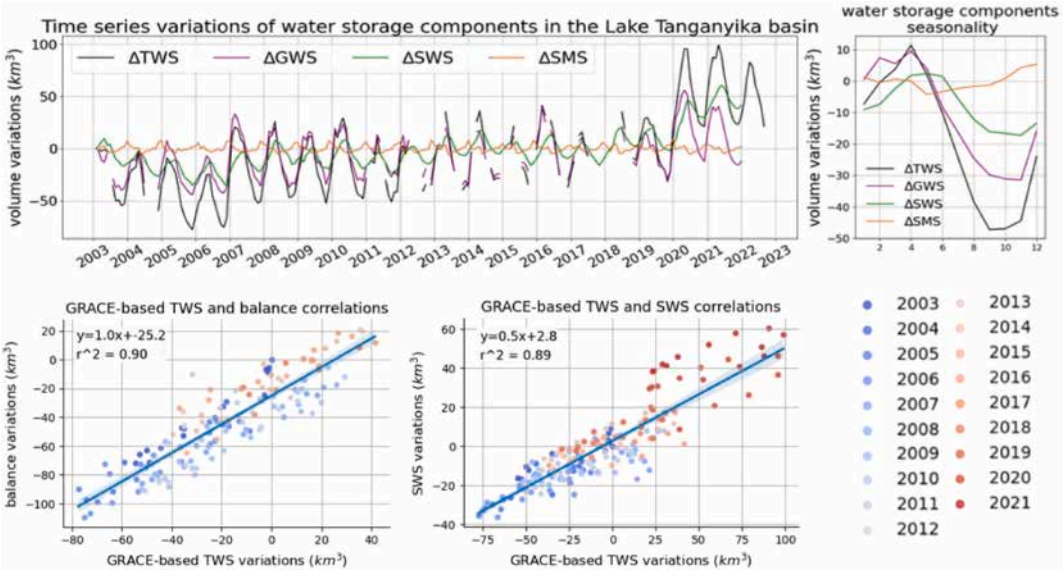

Fig. 5. Time series of water balance components (top left) and their seasonality (top right). Correlations between GRACE-based TWS and water balance (bottom left), and between GRACE-based TWS and SWS (bottom right).

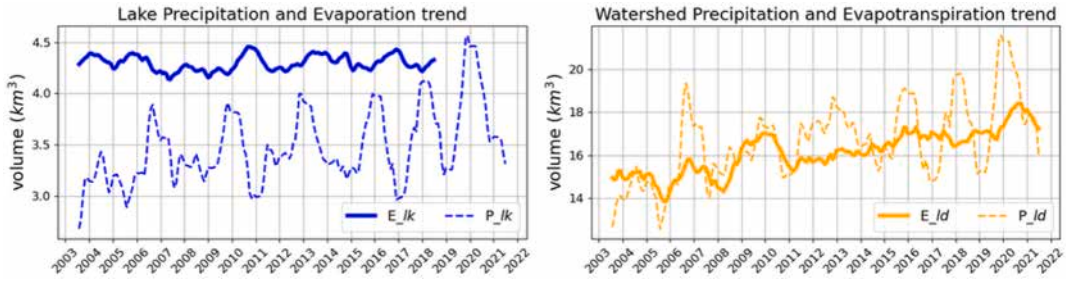

Fig. 6. Lake precipitation (P_*lk*) and E (E_*lk*) trends (left); watershed precipitation (P_*ld*) and E (E_*ld*) trends (right).

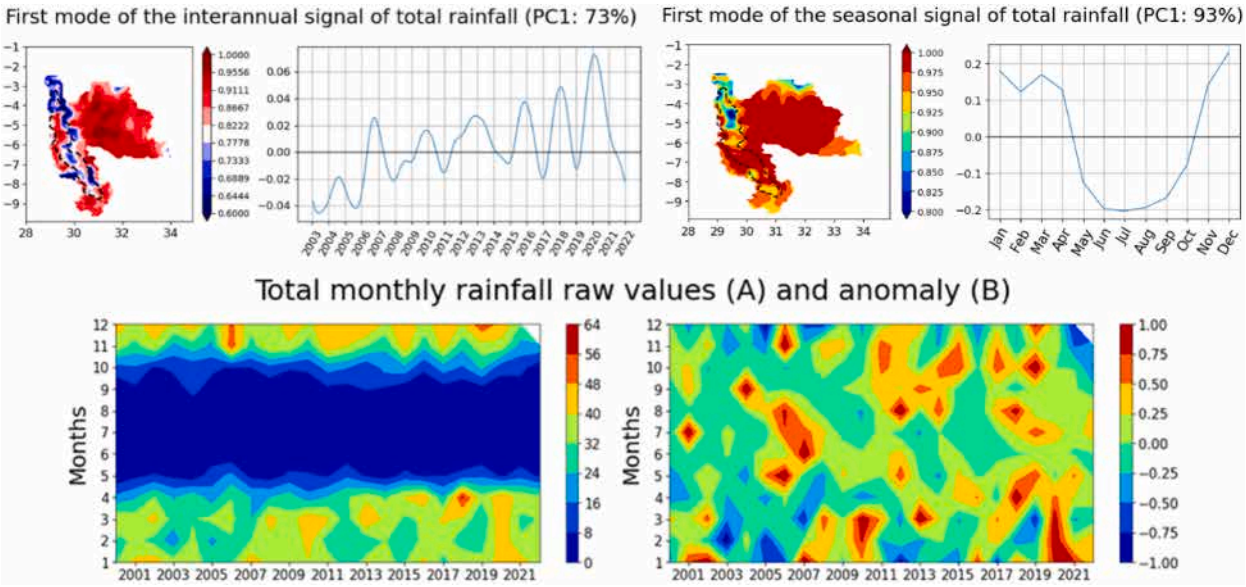

Fig. 7. The first modes of the spatiotemporal variability in the seasonal (top left) and interannual (top right) rainfall signals in the lake watershed. For each mode, the EOF (map) corresponds to the weight of the PC (curve), and both components represent the variance. For the top left panel, PC1, which represents the seasonal mean rainfall variance, was obtained by averaging the monthly values between 2003 and 2021. The bottom panel shows the raw values (left) and the anomalies (right) for total monthly rainfall in the watershed.

or less uniform with P_*lk* and P_*ld* trends. However, the spatial distribution of variances in EOF1 showed that the increase in rainfall was more pronounced in the Malagarasi basin and in the mountains in the southern half of the lake shores (EOF1 $>$ 0.8).

These trends indicate the least rainy years (2003 and 2005) and the wettest years (2006, 2015, 2017, 2019, and 2020). For this observation period, the rainfall anomalies and their seasonality explained at 93% by the first mode of the seasonal signal allowed us to understand these differences. Indeed, in a given year, ~97% of the annual sum of precipitation was recorded from January to May and October to December, with maxima registered in December (Fig. 7). Since all the variances explained by the EOF1 of the seasonal and intraseasonal variabilities were positive, this seasonality of the rainfall plotted by the PC1 was common throughout the watershed.

Therefore, the least rainy years are those with significant negative rainfall anomalies during the rainy season, such as February–April and November–December in 2003 or January–February and November–December in 2005. On the other hand, in 2006, 2010 and 2020, for example, the positive anomalies recorded during the rainy season between November and December, between January and March, and between January and May, respectively, increased the annual sum of rainfall in these years (in Fig. 2 the PEra_EMod balance differs from that of PImerg_EMod according to the estimates of rainfall in 2006–2007 and 2009–2010). This suggests that, for these years, the excess precipitation corresponds to an increase in the total rainfall during the rainy season and not to an extension of the rainy season.

The above results showed that rainfall from ERA5 combined with E and ET from GLEV and MOD16A2, respectively, corresponded to Lake Tanganyika TWS variations and closed the basin water balance. Groundwater stored 57.7% of the basin's total water. For the 2003–2021 period, increased rainfall and ET influenced the water balance. Rainfall increases were greatest in the Malagarasi watershed. The strong variability in the water balance of the Lake Tanganyika basin, with high episodes of rainfall in the watershed leading to a high rise in the lake level in a region with a dense population along the lake shores, has potentially disastrous consequences, as analyzed in the following section.

3.2. Consequences of lake water level variations on lake shores and the surrounding land

The Ruzizi Delta Nature Reserve and the Ruzizi River mouth, which drains water from Lake Kivu into Lake Tanganyika, are located on the northern shores of Lake Tanganyika. These shores are also among the most urbanized boundaries of Lake Tanganyika. Indeed, there are cities such as Bujumbura (Burundi's capital) or Gatumba on the Burundi side and Uvira in the DRC. This area, therefore, provides the necessary assets to study the vulnerability of lake shores and nearby lowland areas to observed variations in lake water levels.

Over a year, soils are more flooded in May (the maximum ΔSWS also occurs in May), and according to their time series, their proportion increases significantly from 2020 onward (Fig. 8). These interannual dynamics, comparable to those of the TWS and SWS (Fig. 5), showed that increases in TWS are followed by rising water levels in the lake shores and the surrounding land.

Fig. 8 illustrates these changes, through the MNDWI's May maps for each year (for years when May satellite images were available) when soil immersion was highest. It was clear based on these maps that flooding of wetlands, flooding of the urban areas surrounding the lake hinterland, and the recession of the coastline are the two major phenomena resulting from the increase in the lake water level in this specific area.

3.2.1. Flooding of the urban areas

At the boundary between southern Gatumba and northern Ruzizi Delta Nature Reserve, on the left bank of the Ruzizi River, soil immersion started to occur in 2018. This immersion became significant beginning in 2020, the maximum occurred in 2021, and then the immersion regressed slightly in 2022, though remained high. The right bank was also subject to the same changes, particularly in 2020 and 2021, with a maximum water level increase occurring in 2021.

3.2.2. Flooding of wetlands and recession of the coastline

In the Ruzizi Delta Nature Reserve, the consequences of the increases in the lake's level were mainly materialized by the gradual increase in the water surfaces in its central region beginning in 2017. The maps in Fig. 8 also show gradual shoreline loss along the entire width of the northern shores of the lake. This phenomenon intensified from 2020 onward and manifested itself, especially in the progressive flooding of the southern border of the Ruzizi Delta Nature Reserve.

4. Discussion

4.1. Comparison of space–time water dynamics

4.1.1. Differences between the obtained water balance and the previous hydrological budget

The monthly level variations in Lake Tanganyika from 1845 to 1995 were compiled with multiyear data on lake E, precipitation, tributaries and outlet flow by Branchu and Bergonzini (2004) to compute the lake's annual hydrological budget (Table 1). In this table, we compare these earlier results with the lake direct rainfall (P_*lk*) and E (E_*lk*) data we found from 2003 to 2021, as well as the runoff data we used (2003–2020). This comparison highlighted that PChirps and PMswep rainfalls were lower than previously reported, while PEra, PImerg and PGsmap were at least ~4 km^3/year greater. E values were lower since GLEV E, the closest to the previ-

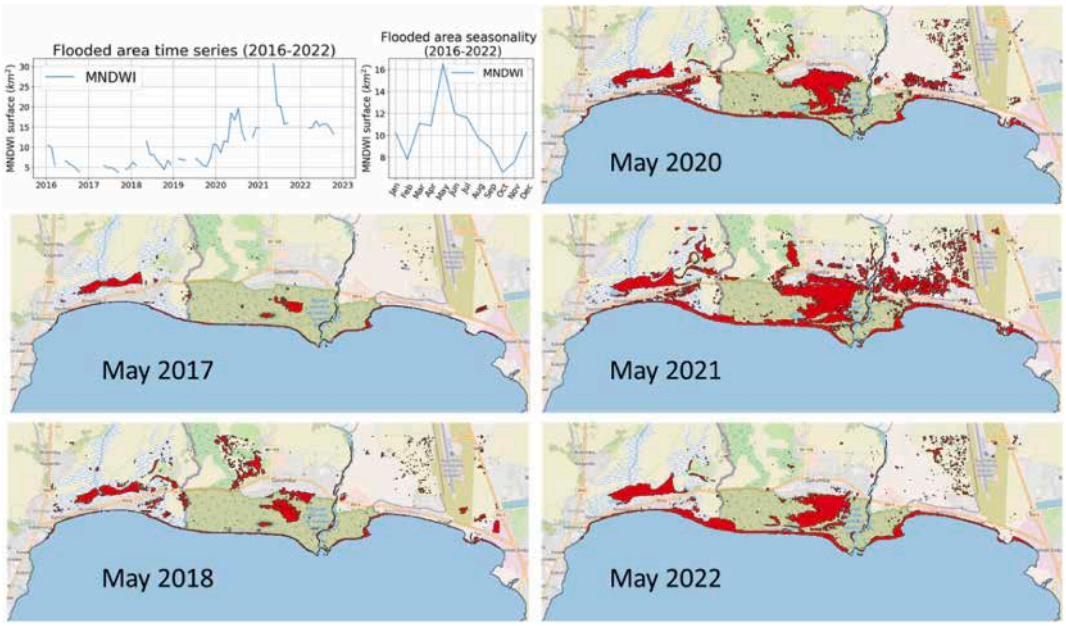

Fig. 8. Flooded area time series and seasonality (top left) and their spatial distribution (2017, 2018, 2020, 2021, 2022). The time series is incomplete, and there is no image for May 2019, because only satellite images with cloud cover <20% were selected for this calculation.

Table 1
Comparison of the annual hydrological budget of Lake Tanganyika.

	Branchu and Bergonzini (2004)	Our study				
Precipitation (km^3/year)	35.5	PEra	PChirps	PGsmap	PImerg	PMswep
		41.3	29.42	39.1	42.24	25.53
E (km^3/year)	55.3	GLEV (2003–2018)	EEra			
		51.55	40.37			
Tributaries (km^3/year)	29.5	9.97 (only Ruzizi + Malagarasi)				
Outlet (km^3/year)	9.7	2.45				

ous one, was ~3.7 km^3/year lower and ERA5 was ~15 km^3/year lower. The annual sum of Ruzizi and Malagarasi discharge over the 2003–2020 period (which does not include runoff from the surrounding mountains along the lake) used in this study to estimate total runoff in the watershed is ~20 km^3/year lower than previously reported tributary values. Concerning the outlet, the difference between the two was ~7 km^3/year. These comparisons revealed significant differences between the hydrological budget inputs for the two periods (1845–1995 and 2003–2020), but these differences had no influence on the TWS study. First, discharge values have a lower order of magnitude than the other components of the hydrological budget; second, only the TWS variations internal to the basin are considered in this study.

For the Branchu and Bergonzini (2004) hydrological budget, the lake water input from precipitation was equal to the watershed runoff, with E accounting for 85% of the total water loss. We found that with the PEra_EMod combination, which closed the hydrological balance, rainfall represented 80.55% of the total water input to the lake, and E represented 95.45% of the water output, which is similar to the results of Branchu and Bergonzini (2004).

On the interannual time scale, lake E has remained stable, but rainfall has increased significantly. These dynamics, combined with upward trends in ET and rainfall over the rest of the watershed after a slight drop between 2003 and 2006, resulted in a water balance for the basin (also corresponding to basin ΔTWS), which decreased between 2003 and 2006 and increased from 2007 onward. The temporal variations in TWS GRACE-based data in the Lake Tanganyika basin highlighted by this study are consistent with the findings of Seka et al. (2022), who studied TWS variation in the East African region and showed an overall increase in TWS GRACE-based data in the Victoria, Tanganyika, Turkana, Abaya-Chamo and Tana basins by applying a Mann–Kendall correlation to annual TWS values in these basins. The same GRACE-derived TWS trends were found by Seka et al. (2022) in this region.

4.1.2. Influence of rainfall and other climate variables on ΔTWS

Becker et al. (2010) and Forootan et al. (2019) showed that rainfall is one of the main factors affecting the observed dynamics of TWS. Hassan and Jin (2014) supported this observation by showing lags of approximately 2.21, 2.25, and 2.3 months in TWS GRACE-based variations in response to TRMM rainfall changes in the Lakes Victoria, Tanganyika and Malawi basins, respectively. In this region, rainfall and GRACE-based TWSs share common interannual dynamics and are strongly controlled by the Indian Ocean Dipole and the El Nino-Southern Oscillation cycle (Becker et al., 2010; Scanlon et al., 2022). Seka et al. (2022) added runoff, ET, and temperature as other climate drivers of TWS changes at the East African region scale and demonstrated that, in contrast to precipitation, increasing ET and temperature lead to reduced TWS. Our study showed increasing trends in rainfall in the Lake Tanganyika basin, mainly in the Malagarasi catchment, and Fig. 6 shows that in 2020, the rainfall was probably greater than that in lake E, which probably contributed to flooding.

4.2. Early warning of floods

Early flood warning systems can be very useful in flood-prone areas to reduce risk by providing early and accurate warnings of flood hazards to a variety of users. This approach helps public actors, humanitarians organizations and other organizations rapidly evacuate goods and people and reduce loss of life and property destruction. In this study, the one-month delay in the ΔSWS response to the ΔTWS, shown in the previous sections, was investigated for this purpose. The ΔTWS reaches its maximum in April, whereas the ΔSWS reaches its maximum in May when flooding is at its worst (Fig. 5). As the ΔSWS is strongly and positively correlated with the ΔTWS, with a correlation coefficient of 0.91, we then calculated the linear regression between these two variables to estimate the May ΔSWS variation as a function of the observed April ΔTWS.

However, with April's ΔTWS and May's ΔSWS, the early warning period was only one month. We then extended this period by an additional two months, correlating the February and March ΔTWSs with the May ΔSWS. The aim is to warn various stakeholders (planners and victims) as early as possible. For these correlations, the ΔTWS results from Equation (1) and the ΔSWS from Equation (3) were used as observed values. The three regressions were calibrated between 2003 and 2020 so that they could be tested to estimate the strong variations in 2021 and 2022. In 2021 and 2022, the observed May ΔSWS values were 60.7 km^3 and 54.06 km^3, respectively.

4.2.1. Estimated values of ΔSWS

The regression with April's ΔTWS is the most correlated with May's ΔSWS with an R^2 of 0.95, followed by the regression with March's ΔTWS with an R^2 of 0.94 and the regression with February's ΔTWS with an R^2 of 0.85 (Fig. 9). Concerning the estimated ΔSWS in May 2021, the forecast with the ΔTWS in April resulted in 46.8 km^3, which was closest to the observed ΔSWS in May, followed by the forecast with the February ΔTWS (46.5 km^3) and the forecast with the March ΔTWS (43.9 km^3). However, in 2022, the

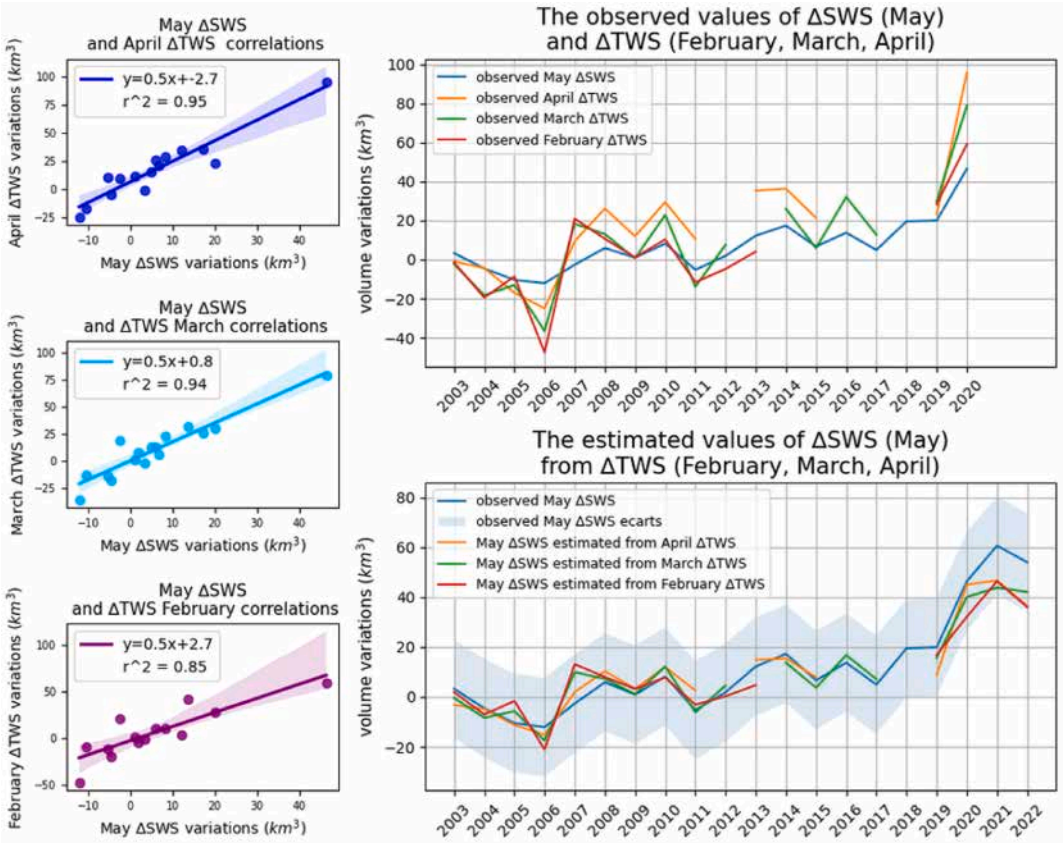

Fig. 9. ΔSWS estimations in May. The three panels on the left represent the correlations between the ΔSWS observed in May and the ΔTWS in April, March and February from top to bottom. The top right panel shows the time series of ΔSWS in May and the observed ΔTWS values (April, March, and February). The bottom right panel shows the time series of the predicted May ΔSWS.

estimation with ΔTWS in March (42.2 km^3) was closest to the observed values of the May ΔSWS, followed by the estimation with ΔTWS in April (36.6 km^3) and the estimation with ΔTWS in February (36.09 km^3).

4.2.2. Correlation assessments and findings

The RMSEs between the ΔSWS observed in May and the values estimated from the ΔTWS in April, March and February were 6.9 km^3, 6.5 km^3, and 9.08 km^3, respectively. The estimates of ΔSWS in May are within the deviation (Fig. 9), and the differences from the observed values in 2021 and 2022 are ~14 and 18 km^3 for the estimation with ΔTWS in February, 17 and 12 km^3 for the estimation with March, and 14 and 18 km^3 for the estimation with April.

These results, which show significant variations in TWS, are early warnings of flooding. This approach can help to develop a massive flood management policy that anticipates floods approximately 3 months in advance to limit the loss of property and human life. However, these results can be improved with a larger number of observations. Indeed, the observed time series of ΔTWS were incomplete, particularly between 2011 and 2019. Over the calibration period from 2003 to 2020, there were only two extremes (2006 and 2019), and the observed ΔTWS amplitude was 60 km^3. The analysis does not allow us to establish a flood forecasting system, but it allows us to understand the linkage between the ΔSWS at different seasons of the year and the resulting flood along the lake's shoreline.

5. Conclusion

This study computed the Lake Tanganyika basin water budget for the period 2003–2021. The basin water flux calculated by combining five different rainfall datasets (IMERG, GSMAP, ERA5, CHIRPS, and MSWEP) with E and ET datasets (GLEV, MODIS, and ERA5) was compared to the variations in the watershed TWS derived from GRACE data. The combination of rainfall from ERA5 with E and ET from GLEV and MOD16A2, respectively, was the most strongly correlated (0.89) with GRACE-based TWS variations and therefore closed the basin water balance. Over the Lake Tanganyika basin, during the 2003–2018 period, water losses of ~70 km^3 due to lake E were offset by an increase in water inflows of ~100 km^3 in the rest of the watershed. The temporal variability in GRACE-based TWS as well as the basin water budget highlighted a decreasing trend during the 2003–2005 period when ET was greater than rainfall and an increasing trend from 2006 onward when rainfall exceeded ET. The change in water volume in the basin's main reservoirs was also investigated. Over the observed period (2003–2021), groundwater storage corresponds to ~57.7% of the GRACE-based TWS and SWS to 41.8%, whereas SMS corresponds to less than 0.5% of the GRACE-based TWS. Investigating land use and land cover

changes in watershed (e.g., vegetation cover, agricultural spread, etc.) can also provide further explanations for these observed dynamics. For example, changes in the land surface as a result of reduced vegetation cover or intensification of agricultural activity can affect soil moisture by increasing soil evaporation and reducing water infiltration (Liao et al., 2021; Regüés et al., 2017).

To describe the exposure of surrounding lowlands to flooding on the northern shores of the lake, the MNDWI was calculated from Sentinel–2 images acquired in May (between 2017 and 2022) when soil immersion was highest, allowing us to map the distribution of soils submerged by the observed variations in lake water level. The results revealed the recession of the coastline and the flooding of urban areas surrounding the lake hinterland, as well as wetlands, particularly in the Ruzizi Delta Nature Reserve. The impact of these changes on wildlife, particularly in the Ruzizi Delta Nature Reserve, also needs to be explored.

Correlating GRACE-based TWS variations with SWS variations highlights that, significant variations in TWS are an early warning of flooding. This correlation allowed us to estimate the SWS in May when the flood risk was the highest, using TWSs in February, March and April with accuracies of 85%, 94% and 95%, respectively. These results provide valuable information for investigating the potential of TWS variations for flood modeling and may also help improve flood prediction models elsewhere in the world where rising lake levels are the cause of flooding leading to significant damage. For flood early warning systems, we chose not to interpolate the data to fill in missing values in order to work with the raw values. This is why we have few variations, mainly for the 2011 to 2019 period. For the study of different lakes around the world, it would be interesting to test the approach based on TWS variations using GRACE data to determine whether additional variations can improve flood forecasts.

Funding

This work was funded by the ESA Climate Change Initiative project on the Lake Essential Climate Variables (Contract No. 40000125030/18/I-NB).

CRediT authorship contribution statement

Paul Gérard Gbetkom: Writing – original draft, Software, Methodology, Conceptualization. **Jean-François Crétaux:** Writing – original draft, Validation, Supervision, Methodology, Funding acquisition, Conceptualization. **Sylvain Biancamaria:** Writing – original draft, Validation, Supervision, Methodology, Conceptualization. **Alejandro Blazquez:** Software, Methodology. **Adrien Paris:** Software, Methodology. **Michel Tchilibou:** Software, Methodology. **Laetitia Gal:** Software, Methodology. **Benjamin Kitambo:** Software, Methodology. **Rômulo Augusto Jucá Oliveira:** Software, Methodology. **Marielle Gosset:** Writing – original draft, Validation, Supervision.

Declaration of competing interest

The authors declare that they have no known competing financial interests or personal relationships that could have appeared to influence the work reported in this paper.

Data availability

Data will be made available on request.

Acknowledgments

The authors are grateful to Hydro Matters for providing the Lukuga, Malagarasi and Ruzizi discharge data. We are grateful to LEGOS and CLS for providing the altimetry database in a standard and suitable form via the Hydroweb project. The authors also thank ESA for the Sentinel–2 data, NASA and DLR for the GRACE data, ECMWF for the ERA5-Land data, NASA for the MODIS and GLDAS-CLSM images, Gang Zhao, Yao Li, Liming Zhou and Huilin Gao for the GLEV data, the precipitation dataset producers, and the FABDEM data producers.

Appendix A. Supplementary data

Supplementary data to this article can be found online at https://doi.org/10.1016/j.rsase.2024.101182.

References

Allasia, D., Silva, B., Silva, D., Collischonn, W., Eduardo, C., Tucci, C., 2006. Large Basin Simulation Experience in South America. IAHS-AISH Publ.

Awange, J.L., Saleem, A., Sukhadiya, R.M., Ouma, Y.O., Kexiang, H., 2019. Physical dynamics of Lake Victoria over the past 34 years (1984–2018): is the lake dying? Sci. Total Environ. 658, 199–218. https://doi.org/10.1016/j.scitotenv.2018.12.051.

Bathelemy, R., Brigode, P., Boisson, D., Tric, E., 2022. Rainfall in the Greater and Lesser Antilles: performance of five gridded datasets on a daily timescale. J. Hydrol. Reg. Stud. 43, 101203. https://doi.org/10.1016/j.ejrh.2022.101203.

Beck, H.E., Wood, E.F., Pan, M., Fisher, C.K., Miralles, D.G., Van Dijk, A.I.J.M., McVicar, T.R., Adler, R.F., 2019. MSWEP V2 global 3-hourly 0.1° precipitation: methodology and quantitative assessment. Bull. Am. Meteorol. Soc. 100, 473–500. https://doi.org/10.1175/BAMS-D-17-0138.1.

Becker, M., Llovel, W., Cazenave, A., Güntner, A., Crétaux, J.-F., 2010. Recent hydrological behavior of the East African great lakes region inferred from GRACE, satellite altimetry and rainfall observations. Compt. Rendus Geosci. 342, 223–233. https://doi.org/10.1016/j.crte.2009.12.010.

Biancamaria, S., Mballo, M., Le Moigne, P., Sánchez Pérez, J.M., Espitalier-Noël, G., Grusson, Y., Cakir, R., Häfliger, V., Barathieu, F., Trasmonte, M., Boone, A., Martin, E., Sauvage, S., 2019. Total water storage variability from GRACE mission and hydrological models for a 50,000 km2 temperate watershed: the Garonne River basin (France). J. Hydrol. Reg. Stud. 24, 100609. https://doi.org/10.1016/j.ejrh.2019.100609.

Blazquez, A., Meyssignac, B., Lemoine, J., Berthier, E., Ribes, A., Cazenave, A., 2018. Exploring the uncertainty in GRACE estimates of the mass redistributions at the

Earth surface: implications for the global water and sea level budgets. Geophys. J. Int. 215, 415–430. https://doi.org/10.1093/gji/ggy293.
Branchu, Ph, Bergonzini, L., 2004. Chloride concentrations in Lake Tanganyika: an indicator of the hydrological budget? Hydrol. Earth Syst. Sci. 8, 256–265. https://doi.org/10.5194/hess-8-256-2004.
Carrea, L., Crétaux, J.-F., Liu, X., Wu, Y., Calmettes, B., Duguay, C.R., Merchant, C.J., Selmes, N., Simis, S.G.H., Warren, M., Yesou, H., Müller, D., Jiang, D., Embury, O., Bergé-Nguyen, M., Albergel, C., 2023. Satellite-derived multivariate world-wide lake physical variable timeseries for climate studies. Sci. Data 10, 30. https://doi.org/10.1038/s41597-022-01889-z.
Che, X., Zhang, H.K., Sun, Q., Ouyang, Z., Liu, J., 2022. MODIS evapotranspiration downscaling using a deep neural network trained using Landsat 8 reflectance and temperature data. Rem. Sens. 14, 5876. https://doi.org/10.3390/rs14225876.
Collischonn, W., Allasia, D., Da Silva, B.C., Tucci, C.E.M., 2007. The MGB-IPH model for large-scale rainfall—runoff modelling. Hydrol. Sci. J. 52, 878–895. https://doi.org/10.1623/hysj.52.5.878.
Conway, D., 2002. Extreme rainfall events and Lake level changes in East Africa: recent events and historical precedents. In: Odada, E.O., Olago, D.O. (Eds.), The East African Great Lakes: Limnology, Palaeolimnology and Biodiversity, Advances in Global Change Research. Springer Netherlands, Dordrecht, pp. 63–92. https://doi.org/10.1007/0-306-48201-0_2.
Crétaux, J., Jeliński, W., Calmant, S., Kouraev, A., Vuglinski, V., Bergé-Nguyen, M., Gennero, M., Niño, F., Rio, R.A., Cazenave, A., Maisongrande, P., 2011. SOLS: A Lake Database to Monitor in the Near Real Time Water Level and Storage Variations from Remote Sensing Data. https://doi.org/10.1016/J.ASR.2011.01.004.
Crétaux, J.-F., Abarca-del-Río, R., Bergé-Nguyen, M., Arsen, A., Drolon, V., Clos, G., Maisongrande, P., 2016. Lake volume monitoring from space. Surv. Geophys. 37, 269–305. https://doi.org/10.1007/s10712-016-9362-6.
Crétaux, J.-F., Birkett, C., 2006. Lake studies from satellite radar altimetry. Compt. Rendus Geosci. 338, 1098–1112. https://doi.org/10.1016/j.crte.2006.08.002.
Crétaux, J.-F., Calmant, S., Romanovski, V., Shabunin, A., Lyard, F., Bergé-Nguyen, M., Cazenave, A., Hernandez, F., Perosanz, F., 2009. An absolute calibration site for radar altimeters in the continental domain: lake Issykkul in Central Asia. J. Geodyn. 83, 723–735. https://doi.org/10.1007/s00190-008-0289-7.
Darwall, W.R.T., Lowe, T., Smith, K.G., Vié, J.-C., 2005. The Status and Distribution of Freshwater Biodiversity in Eastern Africa. IUCN.
Degano, M.F., Rivas, R.E., Carmona, F., Niclòs, R., Sánchez, J.M., 2021. Evaluation of the MOD16A2 evapotranspiration product in an agricultural area of Argentina, the Pampas region. Egypt. J. Remote Sens. Space Sci. 24, 319–328. https://doi.org/10.1016/j.ejrs.2020.08.004.
Deus, D., Gloaguen, R., 2013. Remote Sensing Analysis of Lake Dynamics in Semi-arid Regions: Implication for Water Resource Management. Lake Manyara, East African Rift, Northern Tanzania.
Dokulil, M.T., De Eyto, E., Maberly, S.C., May, L., Weyhenmeyer, G.A., Woolway, R.I., 2021. Increasing maximum lake surface temperature under climate change. Clim. Change 165, 56. https://doi.org/10.1007/s10584-021-03085-1.
Famiglietti, J.S., Lo, M., Ho, S.L., Bethune, J., Anderson, K.J., Syed, T.H., Swenson, S.C., De Linage, C.R., Rodell, M., 2011. Satellites measure recent rates of groundwater depletion in California's Central Valley. Geophys. Res. Lett. 38, 2010GL046442. https://doi.org/10.1029/2010GL046442.
Fathian, F., Dehghan, Z., Eslamian, S., 2014. Analysis of water level changes in Lake Urmia based on data characteristics and non-parametric test. Int. J. Hydrol. Sci. Technol. 4, 18. https://doi.org/10.1504/IJHST.2014.064398.
Fedotova, E., Gosteva, A., 2021. Using of Google earth engine in monitoring systems. E3S Web Conf 333, 01013. https://doi.org/10.1051/e3sconf/202133301013.
Forootan, E., Khaki, M., Schumacher, M., Wulfmeyer, V., Mehrnegar, N., Van Dijk, A.I.J.M., Brocca, L., Farzaneh, S., Akinluyi, F., Ramillien, G., Shum, C.K., Awange, J., Mostafaie, A., 2019. Understanding the global hydrological droughts of 2003–2016 and their relationships with teleconnections. Sci. Total Environ. 650, 2587–2604. https://doi.org/10.1016/j.scitotenv.2018.09.231.
Funk, C., Peterson, P., Landsfeld, M., Pedreros, D., Verdin, J., Shukla, S., Husak, G., Rowland, J., Harrison, L., Hoell, A., Michaelsen, J., 2015. The climate hazards infrared precipitation with stations—a new environmental record for monitoring extremes. Sci. Data 2, 150066. https://doi.org/10.1038/sdata.2015.66.
Gatti, A., Bertolini, A., 2015. Sentinel-2 Products Specification Document.
Gbetkom, P.G., Crétaux, J.-F., Tchilibou, M., Carret, A., Delhoume, M., Bergé-Nguyen, M., Sylvestre, F., 2023. Lake Chad vegetation cover and surface water variations in response to rainfall fluctuations under recent climate conditions (2000–2020). Sci. Total Environ. 857, 159302. https://doi.org/10.1016/j.scitotenv.2022.159302.
Geoglam, 2020. East Africa 2020 Flood Impacts on Agriculture.
Hassan, A.A., Jin, S., 2014. Lake level change and total water discharge in East Africa Rift Valley from satellite-based observations. Global Planet. Change 117, 79–90. https://doi.org/10.1016/j.gloplacha.2014.03.005.
Hattermann, T., Nicholls, K.W., Hellmer, H.H., Davis, P.E.D., Janout, M.A., Østerhus, S., Schlosser, E., Rohardt, G., Kanzow, T., 2021. Observed interannual changes beneath Filchner-Ronne Ice Shelf linked to large-scale atmospheric circulation. Nat. Commun. 12, 2961. https://doi.org/10.1038/s41467-021-23131-x.
Hawker, L., Uhe, P., Paulo, L., Sosa, J., Savage, J., Sampson, C., Neal, J., 2022. A 30 m global map of elevation with forests and buildings removed. Environ. Res. Lett. 17, 024016. https://doi.org/10.1088/1748-9326/ac4d4f.
Herndon, K., Muench, R., Cherrington, E., Griffin, R., 2020. An assessment of surface water detection methods for water resource management in the Nigerien sahel. Sensors 20, 431. https://doi.org/10.3390/s20020431.
Herrnegger, M., Stecher, G., Schwatke, C., Olang, L., 2021. Hydroclimatic analysis of rising water levels in the Great rift Valley Lakes of Kenya. J. Hydrol. Reg. Stud. 36, 100857. https://doi.org/10.1016/j.ejrh.2021.100857.
Hersbach, H., Bell, B., Berrisford, P., Hirahara, S., Horányi, A., Muñoz-Sabater, J., Nicolas, J., Peubey, C., Radu, R., Schepers, D., Simmons, A., Soci, C., Abdalla, S., Abellan, X., Balsamo, G., Bechtold, P., Biavati, G., Bidlot, J., Bonavita, M., Chiara, G., Dahlgren, P., Dee, D., Diamantakis, M., Dragani, R., Flemming, J., Forbes, R., Fuentes, M., Geer, A., Haimberger, L., Healy, S., Hogan, R.J., Hólm, E., Janisková, M., Keeley, S., Laloyaux, P., Lopez, P., Lupu, C., Radnoti, G., Rosnay, P., Rozum, I., Vamborg, F., Villaume, S., Thépaut, J., 2020. The ERA5 global reanalysis. Q. J. R. Meteorol. Soc. 146, 1999–2049. https://doi.org/10.1002/qj.3803.
Hongo, P.O., Mulaku, G.C., 2021. Flooding of Lake Nakuru national park and its effects on the resident wildlife. J. Geogr. Inf. Syst. 13, 660–670. https://doi.org/10.4236/jgis.2021.136036.
Hu, K.X., Awange, J.L., Kuhn, M., Nanteza, J., 2021. Inference of the spatio-temporal variability and storage potential of groundwater in data-deficient regions through groundwater models and inversion of impact factors on groundwater, as exemplified by the Lake Victoria Basin. Sci. Total Environ. 800, 149355. https://doi.org/10.1016/j.scitotenv.2021.149355.
Huang, W., Duan, W., Chen, Y., 2022. Unravelling lake water storage change in Central Asia: rapid decrease in tail-end lakes and increasing risks to water supply. J. Hydrol. 614, 128546. https://doi.org/10.1016/j.jhydrol.2022.128546.
IOM, 2021. Thousands in Burundi Affected by the Rising Waters of Lake Tanganyika. BURUNDI.
IOM, 2020. FLASH INFO: GATUMBA FLOODS.
Ivory, S.J., McGlue, M.M., Peterman, C., Baldwin, P., Lucas, J., Cohen, A., Russell, J., Saroni, J., Msaky, E., Kimirei, I., Soreghan, M., 2021. Climate, vegetation, and weathering across space and time in Lake Tanganyika (tropical eastern Africa). Quat. Sci. Adv. 3, 100023. https://doi.org/10.1016/j.qsa.2021.100023.
Ivory, S.J., Russell, J., 2016. Climate, herbivory, and fire controls on tropical African forest for the last 60ka. Quat. Sci. Rev. 148, 101–114. https://doi.org/10.1016/j.quascirev.2016.07.015.
Kayastha, M.B., Ye, X., Huang, C., Xue, P., 2022. Future rise of the Great Lakes water levels under climate change. J. Hydrol. 612, 128205. https://doi.org/10.1016/j.jhydrol.2022.128205.
Khaki, M., Awange, J., 2021. The 2019–2020 rise in Lake Victoria monitored from space: exploiting the state-of-the-art GRACE-FO and the newly released ERA-5 reanalysis products. Sensors 21, 4304. https://doi.org/10.3390/s21134304.
Kimaru, A.N., Gathenya, J.M., Cheruiyot, C.K., 2019. The temporal variability of rainfall and streamflow into Lake Nakuru, Kenya, assessed using SWAT and hydrometeorological indices. Hydrology 6, 88. https://doi.org/10.3390/hydrology6040088.
Kumar, S., Peterslidard, C., Tian, Y., Houser, P., Geiger, J., Olden, S., Lighty, L., Eastman, J., Doty, B., Dirmeyer, P., 2006. Land information system: an interoperable framework for high resolution land surface modeling. Environ. Model. Software 21, 1402–1415. https://doi.org/10.1016/j.envsoft.2005.07.004.
Landerer, F.W., Flechtner, F.M., Save, H., Webb, F.H., Bandikova, T., Bertiger, W.I., Bettadpur, S.V., Byun, S.H., Dahle, C., Dobslaw, H., Fahnestock, E., Harvey, N., Kang, Z., Kruizinga, G.L.H., Loomis, B.D., McCullough, C., Murböck, M., Nagel, P., Paik, M., Pie, N., Poole, S., Strekalov, D., Tamisiea, M.E., Wang, F., Watkins, M.M., Wen, H., Wiese, D.N., Yuan, D., 2020. Extending the global mass change data record: GRACE follow-on instrument and science data performance. Geophys.

Res. Lett. 47, e2020GL088306. https://doi.org/10.1029/2020GL088306.
Li, J., Carlson, B.E., Lacis, A.A., 2013. Application of spectral analysis techniques in the intercomparison of aerosol data: 1. An EOF approach to analyze the spatial-temporal variability of aerosol optical depth using multiple remote sensing data sets. J. Geophys. Res. Atmospheres 118, 8640–8648. https://doi.org/10.1002/jgrd.50686.
Li, Lingjie, Wang, Y., Wang, L., Hu, Q., Zhu, Z., Li, Liping, Li, C., 2022. Spatio-temporal accuracy evaluation of MSWEP daily precipitation over the Huaihe River Basin, China: a comparison study with representative satellite- and reanalysis-based products. J. Geogr. Sci. 32, 2271–2290. https://doi.org/10.1007/s11442-022-2047-9.
Liao, Y., Cao, H.-X., Liu, X., Li, H.-T., Hu, Q.-Y., Xue, W.-K., 2021. By increasing infiltration and reducing evaporation, mulching can improve the soil water environment and apple yield of orchards in semiarid areas. Agric. Water Manag. 253.
Liu, E., Zhu, Y., Calvet, J.-C., Lü, H., Bonan, B., Zheng, J., Gou, Q., Wang, X., Ding, Z., Xu, H., Pan, Y., Chen, T., 2023. Evaluation of Root-Zone Soil Moisture over the Huai River Basin (Preprint). Vadose Zone Hydrology/Uncertainty Analysis. https://doi.org/10.5194/egusphere-2023-1597.
Ma, M., Wang, H., Jia, P., Tang, G., Wang, D., Ma, Z., Yan, H., 2020. Application of the GPM-IMERG products in flash flood warning: a case study in yunnan, China. Rem. Sens. 12, 1954. https://doi.org/10.3390/rs12121954.
Mahamat Nour, A., Vallet-Coulomb, C., Gonçalves, J., Sylvestre, F., Deschamps, P., 2021. Rainfall-discharge relationship and water balance over the past 60 years within the Chari-Logone sub-basins, Lake Chad basin. J. Hydrol. Reg. Stud. 35, 100824. https://doi.org/10.1016/j.ejrh.2021.100824.
Makwinja, R., Kaunda, E., Mengistou, S., Alemiew, T., Njaya, F., Kosamu, I.B.M., Kaonga, C.C., 2021. Lake Malombe fishing communities' livelihood, vulnerability, and adaptation strategies. Curr. Res. Environ. Sustain. 3, 100055. https://doi.org/10.1016/j.crsust.2021.100055.
Marsh, C.B., Harder, P., Pomeroy, J.W., 2023. Validation of FABDEM, a global bare-earth elevation model, against UAV-lidar derived elevation in a complex forested mountain catchment. Environ. Res. Commun. 5, 031009. https://doi.org/10.1088/2515-7620/acc56d.
Ministry of Foreign Affairs of the Netherlands, 2018. Climate Change Profile: East African Great Lakes and Ruzizi Plain.
Mu, Q., Zhao, M., Running, S.W., 2011. Improvements to a MODIS global terrestrial evapotranspiration algorithm. Remote Sens. Environ. 115, 1781–1800. https://doi.org/10.1016/j.rse.2011.02.019.
Muita, R., Gikungu, D., Aura, S., Njogu, A., Ndichu, R., Nyinguro, P., Kiptum, C., 2021. Assessment of Rising Water Levels of Rift Valley Lakes in Kenya: the Role of Meteorological Factors.
Muñoz-Sabater, J., Dutra, E., Agustí-Panareda, A., Albergel, C., Arduini, G., Balsamo, G., Boussetta, S., Choulga, M., Harrigan, S., Hersbach, H., Martens, B., Miralles, D.G., Piles, M., Rodríguez-Fernández, N.J., Zsoter, E., Buontempo, C., Thépaut, J.-N., 2021. ERA5-Land: a state-of-the-art global reanalysis dataset for land applications. Earth Syst. Sci. Data 13, 4349–4383. https://doi.org/10.5194/essd-13-4349-2021.
Ndichu, R., Richard, M., David, G., Samuel, K., Andrew, N., Stella, A., 2022. The effect of planetary orbital motions on the rises of Rift Valley lake levels in East Africa. Curr. Investig. Agric. Curr. Res. 10.
Nicholson, S.E., Yin, X., 2001. Rainfall Conditions in Equatorial East Africa during the Nineteenth Century as Inferred from the Record of Lake Victoria.
Nielsen, K., Stenseng, L., Andersen, O.B., Villadsen, H., Knudsen, P., 2015. Validation of CryoSat-2 SAR mode based lake levels. Remote Sens. Environ. 171, 162–170. https://doi.org/10.1016/j.rse.2015.10.023.
Nigatu, Z.M., Fan, D., You, W., 2021. GRACE products and land surface models for estimating the changes in key water storage components in the Nile River Basin. Adv. Space Res. 67, 1896–1913. https://doi.org/10.1016/j.asr.2020.12.042.
Niyoyitungiye, L., 2019. Limnological Study of Lake Tanganyika, Africa with Special Emphasis on Piscicultural Potentiality. Assam University Silchar. (India).
Ocampo-Marulanda, C., Fernández-Álvarez, C., Cerón, W.L., Canchala, T., Carvajal-Escobar, Y., Alfonso-Morales, W., 2022. A spatiotemporal assessment of the high-resolution CHIRPS rainfall dataset in southwestern Colombia using combined principal component analysis. Ain Shams Eng. J. 13, 101739. https://doi.org/10.1016/j.asej.2022.101739.
Ocha, 2021. Burundi: Situation Report. (4 Jun 2021).
Odada, E.O., Olago, D.O., Bugenyi, F., Kulindwa, K., Karimumuryango, J., West, K., Ntiba, M., Wandiga, S., Aloo-Obudho, P., Achola, P., 2003. Environmental assessment of the East African Rift Valley lakes. Aquat. Sci. - Res. Boundaries 65, 254–271. https://doi.org/10.1007/s00027-003-0638-9.
Pan, M., Yang, K., 2021. Analysis of variation characteristicsand driving factors of tonle sap lake's SurfaceWater temperature from 2001 to 2018. Pol. J. Environ. Stud. 30, 2709–2722. https://doi.org/10.15244/pjoes/129700.
Papa, F., Crétaux, J.-F., Grippa, M., Robert, E., Trigg, M., Tshimanga, R.M., Kitambo, B., Paris, A., Carr, A., Fleischmann, A.S., De Fleury, M., Gbetkom, P.G., Calmettes, B., Calmant, S., 2023. Water resources in Africa under global change: monitoring surface waters from space. Surv. Geophys. 44, 43–93. https://doi.org/10.1007/s10712-022-09700-9.
Pavur, G., Lakshmi, V., 2023. Observing the recent floods and drought in the Lake Victoria Basin using Earth observations and hydrological anomalies. J. Hydrol. Reg. Stud. 46, 101347. https://doi.org/10.1016/j.ejrh.2023.101347.
Pelosi, A., Terribile, F., D'Urso, G., Chirico, G., 2020. Comparison of ERA5-land and UERRA MESCAN-SURFEX reanalysis data with spatially interpolated weather observations for the regional assessment of reference evapotranspiration. Water 12, 1669. https://doi.org/10.3390/w12061669.
Peña-Guerrero, M.D., Umirbekov, A., Tarasova, L., Müller, D., 2022. Comparing the performance of high-resolution global precipitation products across topographic and climatic gradients of Central Asia. Int. J. Climatol. 42, 5554–5569. https://doi.org/10.1002/joc.7548.
Pham-Duc, B., Sylvestre, F., Papa, F., Frappart, F., Bouchez, C., Crétaux, J.-F., 2020. The Lake Chad hydrology under current climate change. Sci. Rep. 10, 5498. https://doi.org/10.1038/s41598-020-62417-w.
Plisnier, P.-D., Nshombo, M., Mgana, H., Ntakimazi, G., 2018. Monitoring climate change and anthropogenic pressure at Lake Tanganyika. J. Gt. Lakes Res. 44, 1194–1208. https://doi.org/10.1016/j.jglr.2018.05.019.
Priyambodoho, B.A., Kure, S., Yagi, R., Januriyadi, N.F., 2021. Flood inundation simulations based on GSMaP satellite rainfall data in Jakarta, Indonesia. Prog. Earth Planet. Sci. 8, 34. https://doi.org/10.1186/s40645-021-00425-8.
Ramadhan, R., Marzuki, M., Yusnaini, H., Muharsyah, R., Tangang, F., Vonnisa, M., Harmadi, H., 2023. A preliminary assessment of the GSMaP version 08 products over Indonesian maritime continent against gauge data. Rem. Sens. 15, 1115. https://doi.org/10.3390/rs15041115.
Regüés, D., Badía, D., Echeverría, M.T., Gispert, M., Lana-Renault, N., León, J., Nadal, M.E., Pardini, G., Serrano-Muela, P., 2017. Analysing the effect of land use and vegetation cover on soil infiltration in three contrasting environments in northeast Spain. Cuadernos Invest. Geogr. 43, 141–169. https://doi.org/10.18172/cig.3164.
Ričko, M., Birkett, C.M., Carton, J.A., Crétaux, J.-F., 2012. Intercomparison and validation of continental water level products derived from satellite radar altimetry. J. Appl. Remote Sens. 6, 061710. https://doi.org/10.1117/1.JRS.6.061710.
Rodell, M., Houser, P.R., Jambor, U., Gottschalck, J., Mitchell, K., Meng, C.-J., Arsenault, K., Cosgrove, B., Radakovich, J., Bosilovich, M., Entin, J.K., Walker, J.P., Lohmann, D., Toll, D., 2004. The global land data assimilation system. Bull. Am. Meteorol. Soc. 85, 381–394. https://doi.org/10.1175/BAMS-85-3-381.
Sacré Regis, M.D., Mouhamed, L., Kouakou, K., Adeline, B., Arona, D., Houebagnon Saint, J.C., Koffi Claude, A.K., Talnan Jean, H.C., Salomon, O., Issiaka, S., 2020. Using the CHIRPS dataset to investigate historical changes in precipitation extremes in west Africa. Climate 8, 84. https://doi.org/10.3390/cli8070084.
Salza, A., 2023. Drought and floods at Lake Turkana: an anomaly for pastoralists? Nomadic Peoples 27, 95–99. https://doi.org/10.3197/np.2023.270106.
Scanlon, B.R., Rateb, A., Anyamba, A., Kebede, S., MacDonald, A.M., Shamsudduha, M., Small, J., Sun, A., Taylor, R.G., Xie, H., 2022. Linkages between GRACE water storage, hydrologic extremes, and climate teleconnections in major African aquifers. Environ. Res. Lett. 17, 014046. https://doi.org/10.1088/1748-9326/ac3bfc.
Scholz, C.A., Cohen, A.S., Johnson, T.C., King, J., Talbot, M.R., Brown, E.T., 2011. Scientific drilling in the Great Rift Valley: the 2005 Lake Malawi scientific drilling project — an overview of the past 145,000years of climate variability in southern hemisphere East Africa. Palaeogeogr. Palaeoclimatol. Palaeoecol. 303, 3–19. https://doi.org/10.1016/j.palaeo.2010.10.030.
Seka, A.M., Zhang, J., Ayele, G.T., Demeke, Y.G., Han, J., Prodhan, F.A., 2022. Spatio-temporal analysis of water storage variation and temporal correlations in the East Africa lake basins. J. Hydrol. Reg. Stud. 41, 101094. https://doi.org/10.1016/j.ejrh.2022.101094.
Springer, A., Lopez, T., Owor, M., Frappart, F., Stieglitz, T., 2023. The role of space-based observations for groundwater resource monitoring over Africa. Surv. Geophys. 44, 123–172. https://doi.org/10.1007/s10712-022-09759-4.
Stager, J.C., Cumming, B., Meeker, L., 1997. A high-resolution 11,400-Yr diatom record from Lake Victoria, East Africa. Quat. Res. 47, 81–89. https://doi.org/10.1006/qres.1996.1863.

Sterckx, K., Delandmeter, P., Lambrechts, J., Deleersnijder, E., Verburg, P., Thiery, W., 2023. The impact of seasonal variability and climate change on lake Tanganyika's hydrodynamics. Environ. Fluid Mech. 23, 103–123. https://doi.org/10.1007/s10652-022-09908-8.

Stoyneva-Gärtner, M.P., Morana, C., Borges, A.V., Okello, W., Bouillon, S., Deirmendjian, L., Lambert, T., Roland, F., Nankabirwa, A., Nabafu, E., Darchambeau, F., Descy, J.-P., 2020. Diversity and ecology of phytoplankton in Lake edward (East Africa): present status and long-term changes. J. Gt. Lakes Res. 46, 741–751. https://doi.org/10.1016/j.jglr.2020.01.003.

Taburet, N., Zawadzki, L., Vayre, M., Blumstein, D., Le Gac, S., Boy, F., Raynal, M., Labroue, S., Crétaux, J.-F., Femenias, P., 2020. S3MPC: improvement on inland water tracking and water level monitoring from the OLTC onboard sentinel-3 altimeters. Rem. Sens. 12, 3055. https://doi.org/10.3390/rs12183055.

Tan, J., Huffman, G.J., Bolvin, D.T., Nelkin, E.J., 2019. Imerg V06: changes to the morphing algorithm. J. Atmos. Ocean. Technol. 36, 2471–2482. https://doi.org/10.1175/JTECH-D-19-0114.1.

Tapley, B.D., Bettadpur, S., Ries, J.C., Thompson, P.F., Watkins, M.M., 2004. GRACE measurements of mass variability in the earth system. Science 305, 503–505. https://doi.org/10.1126/science.1099192.

Tapley, B.D., Watkins, M.M., Flechtner, F., Reigber, C., Bettadpur, S., Rodell, M., Sasgen, I., Famiglietti, J.S., Landerer, F.W., Chambers, D.P., Reager, J.T., Gardner, A.S., Save, H., Ivins, E.R., Swenson, S.C., Boening, C., Dahle, C., Wiese, D.N., Dobslaw, H., Tamisiea, M.E., Velicogna, I., 2019. Contributions of GRACE to understanding climate change. Nat. Clim. Change 9, 358–369. https://doi.org/10.1038/s41558-019-0456-2.

Torabi Haghighi, A., Kløve, B., 2015. A sensitivity analysis of lake water level response to changes in climate and river regimes. Limnologica 51, 118–130. https://doi.org/10.1016/j.limno.2015.02.001.

Toumazou, V., Crétaux, J.-F., 2001. Using a lanczos eigensolver in the computation of empirical orthogonal functions. Mon. Weather Rev. 129, 1243–1250. https://doi.org/10.1175/1520-0493(2001)129<1243:UALEIT>2.0.CO;2.

Unicef, 2021. Democratic Republic of the Congo Annual Humanitarian Situation Report.

VanDeWeghe, A., Lin, V., Jayaram, J., Gronewold, A.D., 2022. Changes in large Lake Water level dynamics in response to climate change. Front. Water 4, 805143. https://doi.org/10.3389/frwa.2022.805143.

Verburga, P., Hecky, R.E., 2009. The physics of the warming of Lake Tanganyika by climate change. Limnol. Oceanogr. 54, 2418–2430. https://doi.org/10.4319/lo.2009.54.6_part_2.2418.

Victor, N., Eric, P., Kyeba, K., 2023. The risk of flooding to architecture and infrastructure amidst a changing climate in Lake Baringo, Kenya. Am. J. Clim. Change 12, 80–99. https://doi.org/10.4236/ajcc.2023.121005.

Vuglinsky, V.S., Cretaux, J.-F., Izmailova, A.V., Gusev, S.I., Berge-Nguyen, M., Calmettes, B., 2023. Comparison and correction of satellite measurements using in-situ observations of lake surface heights: a case study in lake Baikal. Adv. Space Res. 71, 4030–4044. https://doi.org/10.1016/j.asr.2022.12.046.

Wang, N., Yang, J., Zhang, Z., Xiao, Y., Wang, H., He, J., Yi, L., 2023. Analysis of detailed lake variations and associated hydrologic driving factors in a semi-arid ungauged closed watershed. Sustainability 15, 6535. https://doi.org/10.3390/su15086535.

Wongchuig, S., Kitambo, B., Papa, F., Paris, A., Fleischmann, A.S., Gal, L., Boucharel, J., Paiva, R., Oliveira, R.J., Tshimanga, R.M., Calmant, S., 2023. Improved modeling of Congo's hydrology for floods and droughts analysis and ENSO teleconnections. J. Hydrol. Reg. Stud. 50, 101563. https://doi.org/10.1016/j.ejrh.2023.101563.

Woolway, R.I., Kraemer, B.M., Lenters, J.D., Merchant, C.J., O'Reilly, C.M., Sharma, S., 2020. Global lake responses to climate change. Nat. Rev. Earth Environ. 1, 388–403. https://doi.org/10.1038/s43017-020-0067-5.

Xiang, L., Wang, H., Steffen, H., Wu, P., Jia, L., Jiang, L., Shen, Q., 2016. Groundwater storage changes in the Tibetan Plateau and adjacent areas revealed from GRACE satellite gravity data. Earth Planet Sci. Lett. 449, 228–239. https://doi.org/10.1016/j.epsl.2016.06.002.

Xie, C., Zhang, X., Zhuang, L., Zhu, R., Guo, J., 2022. Analysis of surface temperature variation of lakes in China using MODIS land surface temperature data. Sci. Rep. 12, 2415. https://doi.org/10.1038/s41598-022-06363-9.

Xu, H., 2006. Modification of normalised difference water index (NDWI) to enhance open water features in remotely. Int. J. Rem. Sens. 27, 9.

Yao, F., Livneh, B., Rajagopalan, B., Wang, J., Crétaux, J.-F., Wada, Y., Berge-Nguyen, M., 2023. Satellites reveal widespread decline in global lake water storage. Science 380, 743–749. https://doi.org/10.1126/science.abo2812.

Yu, X., Qian, L., Wang, W., Hu, X., Dong, J., Pi, Y., Fan, K., 2023. Comprehensive evaluation of terrestrial evapotranspiration from different models under extreme condition over conterminous United States. Agric. Water Manag. 289, 108555. https://doi.org/10.1016/j.agwat.2023.108555.

Yu, Z., Di, L., Rahman, MdS., Tang, J., 2020. Fishpond mapping by spectral and spatial-based filtering on Google earth engine: a case study in singra upazila of Bangladesh. Rem. Sens. 12, 2692. https://doi.org/10.3390/rs12172692.

Yücel, A., Markovic, M., Atilgan, A., Rolbiecki, R., Ertop, H., Jagosz, B., Ptach, W., Łangowski, A., Jakubowski, T., 2022. Investigation of annual Lake Water levels and water volumes with şen innovation and mann-kendall rank correlation trend tests: example of Lake eğirdir, Turkey. Water 14, 2374. https://doi.org/10.3390/w14152374.

Zen, S., Perona, P., Medina-Lopez, E., 2023. River delta eco-morphodynamics under changing scenarios: the case of Lake Turkana, Kenya. Geomorphology 428, 108640. https://doi.org/10.1016/j.geomorph.2023.108640.

Zhang, G., Yao, T., Shum, C.K., Yi, S., Yang, K., Xie, H., Feng, W., Bolch, T., Wang, L., Behrangi, A., Zhang, H., Wang, W., Xiang, Y., Yu, J., 2017. Lake volume and groundwater storage variations in Tibetan Plateau's endorheic basin. Geophys. Res. Lett. 44, 5550–5560. https://doi.org/10.1002/2017GL073773.

Zhang, G., Yao, T., Xie, H., Yang, K., Zhu, L., Shum, C.K., Bolch, T., Yi, S., Allen, S., Jiang, L., Chen, W., Ke, C., 2020. Response of Tibetan Plateau lakes to climate change: trends, patterns, and mechanisms. Earth Sci. Rev. 208, 103269. https://doi.org/10.1016/j.earscirev.2020.103269.

Zhang, X., Kurbaniyazov, A., Kirillin, G., 2021. Changing pattern of water level trends in eurasian endorheic lakes as a response to the recent climate variability. Rem. Sens. 13, 3705. https://doi.org/10.3390/rs13183705.

Zhao, G., Li, Y., Zhou, L., Gao, H., 2022. Evaporative water loss of 1.42 million global lakes. Nat. Commun. 13, 3686. https://doi.org/10.1038/s41467-022-31125-6.

Zsoter, Cloke, Prudhomme, Harrigan, de Rosnay, Munoz-Sabater, Stephens, 2020. Trends in the GloFAS-ERA5 River Discharge Reanalysis. European Centre for Medium-Range Weather Forecasts, Reading, UK.